Electronic Supplementary Material (ESI) for ChemComm.

Supporting information for

Enriched Switching in a Donor-Acceptor Stenhouse Adduct via Reversible Covalent Bonding

Peng Xuan Zheng, [a] Song Lin Ou, [a] Lei Yu Qu, [a] Ying Zhang, [a] Shi Qing Jiang, [a] Xiang Li, [a] Jun Xiong Wan, [a] Min Zhang, *[b] and Xin Bao **[a]

[a] P. X. Zheng, S. L. Ou, L. Y. Qu, Y. Zhang, X. Li, S. Q. Jiang, J. X. Wan, Prof. X. Bao
School of Chemistry and Chemical Engineering, Nanjing University of Science and Technology, Nanjing
210094, P. R. China; orcid.org/0000-0002-2725-0195;
E-mail: baox199@126.com

[b] Prof. M. Zhang
Faculty of Chemistry, Northeast Normal University, Changchun130024, P. R. China; orcid.org/0000-0001-5842-9107; E-mail: mzhang@nenu.edu.cn

Table of Contents

General

All reagents obtained from commercial sources were used without further purification.

Physical characterizations

The **IR spectra** were recorded on a Perkin-Elmer Spectrum in the range of 4000–600 cm^{-1}. **UV-Vis spectra** were recorded by the THERMO FISHER EVOLUTION220 instrument in the range of 800–200 nm. ^{1}H, ^{13}C, ^{1}H, ^{1}H-COSY, HSQC, and NOESY **NMR spectra** were recorded on Bruker AVANCE III500 (500 MHz for ^{1}H and 125 MHz for ^{13}C) or Bruker Advance III plus 400 (500 MHz for ^{1}H). Chemical shifts for the specific NMR spectra were reported relative to the residual solvent peak. The multiplicities of the signals are denoted by s (singlet), d (doublet), t (triplet), q (quartet), m (multiplet), dd (doublet doublet), dt (doublet triplet), td (triplet doublet) and br (broad signal). **Mass spectrums** were recorded on Thermo Fisher Q Exactive Orbitrap Mass Spectrometer and Thermo Scientific Q Exactive Focus Mass Spectrometer with ESI ionization. The light source utilized in this study was a 300 W Xenon lamp (CEL-HXF 300, Beijing Zhongjiao Aoli Lighting Co., Ltd.) equipped with a 550nm cutoff filter. It operated at a working voltage of 14 V, a working current of 20 A. The sample was placed in a quartz cuvette 20 cm away from the light source. **PXRD pattern** was recorded on a D8 ADVANCE X-ray diffractometer (CuKα radiation, λ=0.154056 nm). **Single crystal X-ray diffraction.** Single-crystal X-ray data were collected on a Bruker D8 Quest diffractometer using graphite monochromated Mo-Kα radiation (λ= 0.71073 Å). A multi-scan absorption correction was performed (SADABS, Bruker, 2016). The structures were solved using the direct method (SHELXS) and refined by full-matrix least-squares on F^2 using SHELXL[1]under the graphical user interface of Olex2[2]. Non-hydrogen atoms were refined anisotropically, and hydrogen atoms were placed in calculated positions refined using idealized geometries (riding model) and assigned fixed isotropic displacement parameters. CCDC 2204731 contains the supplementary crystallographic data for this paper. The data can be obtained free of charge from The Cambridge Crystallographic Data Centre via www.ccdc.cam.ac.uk/data_request/cif.

1. Syntheses

1.1 Synthesis of 1a

1a

5-((2*Z*,4*E*)-2-hydroxy-5-((2-hydroxyethyl)(methyl)amino)penta-2,4-dien-1-ylidene)-2,2-dimethyl-1,3-dioxane-4,6-dione (**1a**):

5-(furan-2-ylmethylene)-2,2-dimethyl-1,3-dioxane-4,6-dione[3] (0.222 g, 1 mmol) was dissolved in 5 ml tetrahydrofuran. To this solution was added 2-(methylamino)ethanol (0.075 g, 1 mmol). The mixture was stirred at room temperature for 10 min followed by cooling at 0 °C for 20 min. The reaction mixture was then filtered to collect the precipitated solid. The solid was washed with cold diethyl ether and dried in vacuo to afford Stenhouse adduct **1a** (0.256 g, 86.1%) as a red solid. ^{1}H NMR (500 MHz, DMSO-d_6): two sets of signals coexist with a ratio of ~1:3 due to stereoisomers[4]. ^{1}H NMR (500 MHz, DMSO-d_6) δ 11.38 (s, 1H), 8.06 (d, J = 11.6 Hz, 1H) ,7.10 (d, J = 12.3 Hz, 1H), 6.55(s, 1H), 6.19 (t, J = 12.3 Hz, 1H) 7.96 (d, J = 11.6 Hz, 1H), 7.17 (d, J = 13.0 Hz, 1H), 6.60 (s, 1H), 6.08 (t, J = 12.3 Hz, 1H), 5.06 (s, 1H), 3.74 – 3.61 (m, 4H), 3.23 (s, 3H), 1.59 (s, 6H). $^{13}C\{^{1}H\}$ NMR (125 MHz, DMSO-d_6) δ 164.76, 164.02, 154.17, 143.75, 131.32,

105.37, 102.64, 85.85, 62.23, 58.07, 45.94, 37.54, 26.47. HRMS (ESI+) calc. for $C_{14}H_{19}O_6N$ [**1a**+Na]$^+$: 320.11046, found: 320.10898.

1.2 Synthesis of 1b

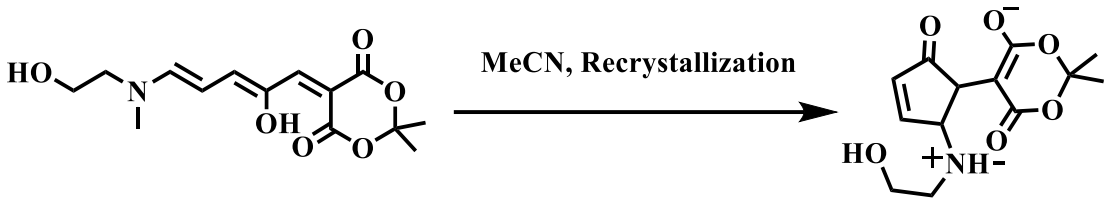

1a **1b**

6-hydroxy-5-(2-((2-hydroxyethyl)(methyl)-l4-azaneyl)-5-oxocyclopent-3-en-1-yl)-2,2-dimethyl-4*H*-1,3-dioxin-4-one(1b):

After recrystallization of crude product **1a** in acetonitrile, a white crystalline powder of **1b** was obtained in 47 % yield. ^{1}H NMR (500 MHz, D_2O) δ 7.81 (d, J = 5.9 Hz, 1H), 6.69 (d, J = 5.9 Hz, 1H), 4.79 – 4.77 (m, 1H), 3.93 (t, J = 4.9 Hz, 2H), 3.65 (d, J = 3.6 Hz, 1H), 3.49 – 3.33 (m, 2H), 2.97 (s, 3H), 1.67 (s, 6H). ^{13}C{^{1}H} NMR (125 MHz, D_2O) δ 208.30, 168.30, 154.80, 138.32, 103.90, 72.89, 70.34, 55.29, 43.78, 37.22, 24.72. HRMS (ESI+) calc. for $C_{14}H_{19}O_6N$ [**1b**+Na]$^+$: 320.11046, found: 320.10889.

1.3 Synthesis of 1d

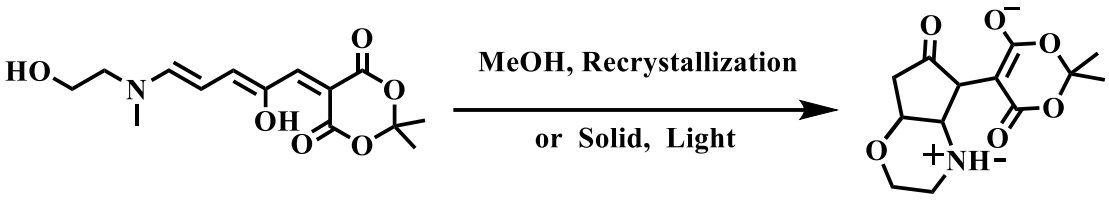

1a **1d**

2,2-dimethyl-5-(4-methyl-6-oxooctahydrocyclopenta[b][1,4]oxazin-4-ium-5-yl)-4-oxo-4*H*-1,3-dioxin-6-olate(1d):

1d can be obtained by solid-state photoisomerization from **1a**: the crystalline powder of **1a** was left to stand in natural light for one month, resulting in the quantitative transformation to **1d** as a yellowish-brown solid. ^{1}H NMR (500 MHz, D_2O) δ 4.63 – 4.58 (m, 1H), 4.24 (d, J = 10.0 Hz, 1H), 4.18 – 4.13 (m, 1H), 3.95 (t, J = 12.3 Hz, 1H), 3.84 (d, J = 10.5 Hz, 1H), 3.54 (t, J = 11.8 Hz, 1H), 3.39 (d, J = 14.3 Hz, 1H), 2.95 (s, 3H), 2.88 (dd, J = 19.1, 4.3 Hz, 1H), 2.62 (d, J = 19.2 Hz, 1H), 1.65 (s, 6H). ^{13}C{^{1}H} NMR (125 MHz, D_2O) δ 216.92, 168.30, 103.89, 74.24, 72.47, 62.72, 46.80, 44.74, 41.25, 24.86. HRMS (ESI+) calc. for $C_{14}H_{19}O_6N$ [**1d**+Na]$^+$: 320.11046, found: 320.10895.

2. UV-Vis absorption spectroscopy and kinetics

2.1 Absorption spectra

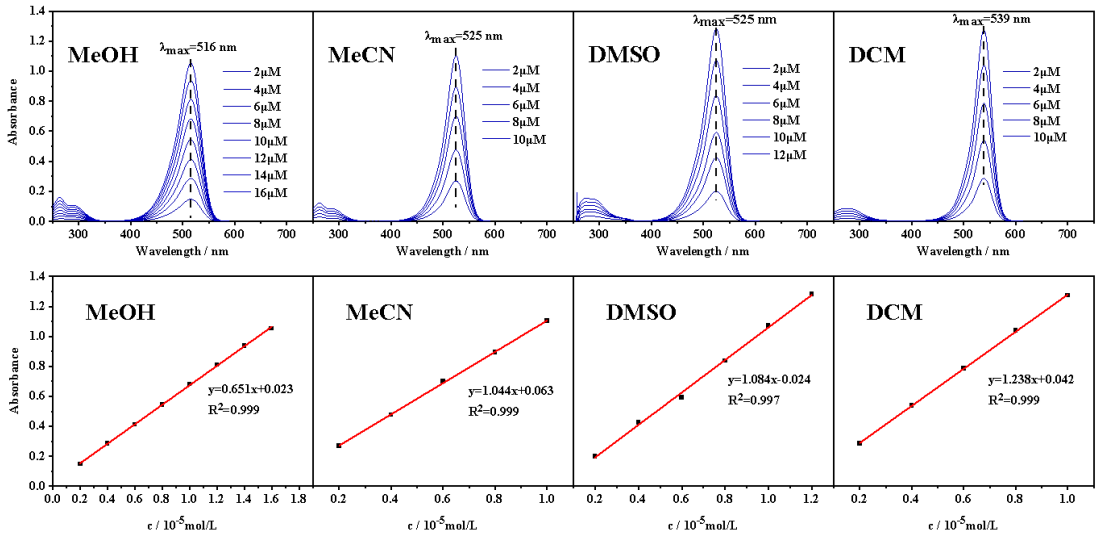

Figure S1. Absorption spectra of **1a** in methanol, acetonitrile, dimethyl sulfoxide, and dichloromethane (top). A linear relationship between the absorbance at λ_{max} and the concentration of **1a** (bottom).

2.2 Solvatochromic shift analysis

Table S1: λ_{max} (nm) values of **1a** in a range of solvents.

Solvent	E_T^N[5]	**1a**-λ_{max}(nm)
Tol	0.099	544
Et_2O	0.117	537
THF	0.207	538
EtOAC	0.228	535
$CHCl_3$	0.259	541
DCM	0.309	539
Acetone	0.355	530
DMSO	0.444	525
ACN	0.460	525
MeOH	0.762	516

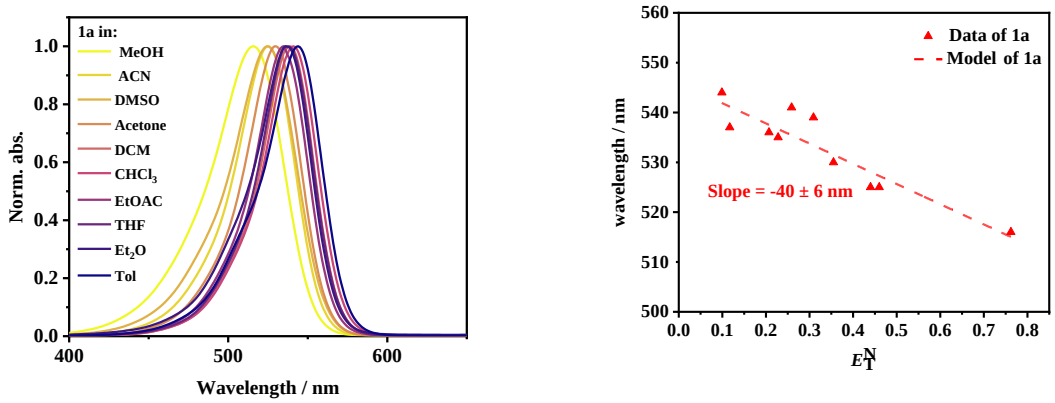

Figure S2. Left: UV-Vis measurements showing the solvatochromic shift of **1a**. Right: Slope of solvatochromic shift.

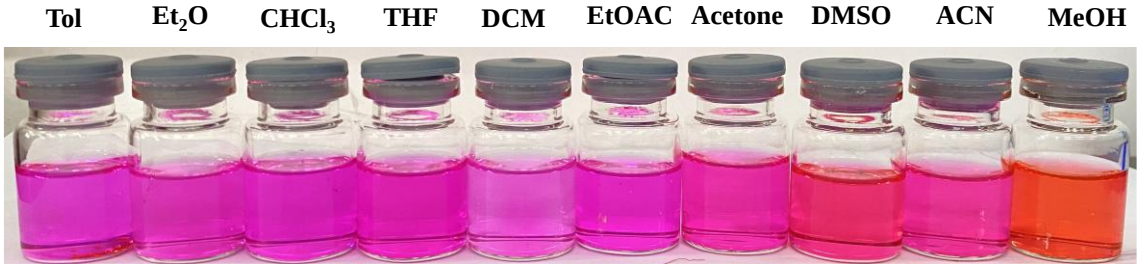

Figure S3. The solvatochromic trends of **1a** (bottom) are visible to the naked eye.

The observed hypsochromic shift in the UV-Vis absorption upon polarity increases of DASA solution is a well documented phenomenon. This phenomenon has been previously reported by various studies, eg. Miranda M. Sroda[6] and Michael M. Lerch [7] et al. The observed changes are related to shift in the extent of charge separation[8].

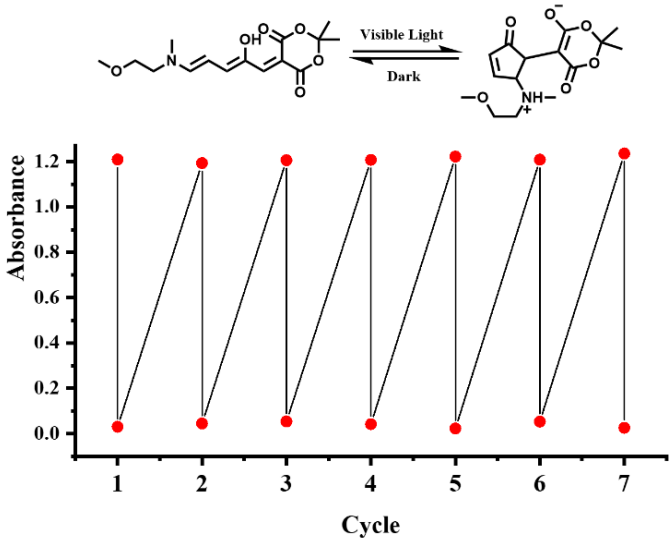

Figure S4. Repeated photoswitching of the DASA as shown in the Figure in toluene (10 µM) with alternative irradiation 550 nm and dark, the absorbance was monitored by UV-Vis spectroscopy at 544 nm.

We observed a photodegradation of **1a** after a few cycles of light irradiation, which we believe is due to further cylization to form **1d** due to Michael addition of OH to cyclopentenone. A replacement of the hydroxyl group by methoxy in the donor can effectively blocks this further isomerization and depressing photodegradation.

2.3 Kinetics

The UV-Vis data was used to determine the apparent half-life times and rate constants of isomerization reactions in toluene under dark conditions.

$$\text{Cyclic form} \underset{k_{-1}}{\overset{k_1}{\rightleftharpoons}} \text{Linear form}$$

Kinetic analysis is performed on the recovery process from cyclic to linear isomer under dark conditions. The differential equation describing the change in concentrations of reactant and product over time (t) can be expressed as follows:

$$\frac{d[cyclic]}{dt} = -k_1[cyclic] + k_{-1}[linear] \quad \text{(S1)}$$

$$\frac{d[linear]}{dt} = -k_{-1}[linear] + k_1[cyclic] \quad \text{(S2)}$$

where $[cyclic]$ and $[linear]$ are the concentrations of the cyclic and linear isomer. The rate constant for the forward reaction (cyclic to linear isomer) is denoted as k_1, while the rate constant for the reverse reaction (linear to cyclic isomer) is denoted as k_{-1}.

According to the principle of mass conservation, $[linear] + [cyclic] = [cyclic]_0$, where $[cyclic]_0$ is the initial concentration of cyclic isomer. This relationship can be represented by incorporating it into formula (S1), yielding the following equation:

$$\frac{d[cyclic]}{dt} = -(k_1 + k_{-1})[cyclic] + k_{-1}[cyclic]_0 \quad \text{(S3)}$$

The integration of the aforementioned formula yields the corresponding solution:

$$[cyclic] = [cyclic]_0 \frac{k_{-1} + k_1 e^{-(k_1 + k_{-1})t}}{k_1 + k_{-1}} \quad \text{(S4)}$$

The simplified form of Formula (S4) represents the relationship between the proportion of cyclic (y_{cyclic}) or linear isomer (y_{linear}) and time (t).

$$y_{cyclic} = \frac{k_{-1} + k_1 e^{-(k_1 + k_{-1})t}}{k_1 + k_{-1}} \quad \text{(S5)}$$

$$y_{linear} = 1 - \frac{k_{-1} + k_1 e^{-(k_1 + k_{-1})t}}{k_1 + k_{-1}} \quad \text{(S6)}$$

To improve the fitting results, we incorporated the time delay constant z and formulated the equation as a function of y_{linear} and time (t):

$$y_{linear} = 1 - \frac{k_{-1} + k_1 e^{-(k_1 + k_{-1})(t+z)}}{k_1 + k_{-1}} \quad \text{(S7)}$$

The half-life $(t_{1/2})$ value was calculated by fitting the curve using an exponential regression analysis. The equation is shown below:

$$y_{linear} = y_0 + Ae^{-R_0 t} \quad \text{(S8)}$$

Where $y_0 = y_{linear}$ offset, $A =$ amplitude, $R_0 =$ rate constant, and $t =$ time in minutes. The half-life is defined as the time required for the fraction of reactants to decrease by half of its initial value:

$$t_{1/2} = \frac{ln2}{R_0} \quad \text{(S9)}$$

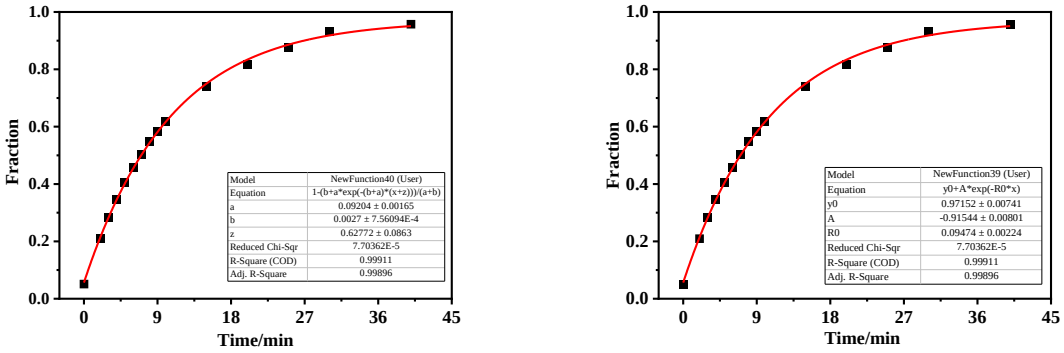

Figure S5. Thermal relaxation of **1a** measured by UV-Vis spectroscopy, giving the apparent half-life time ($t_{1/2}$ = 7.3 min) and rate constants (k_1 = 0.092 and k_{-1} = 0.0027).

3. Dark equilibrium

1a undergoes spontaneous cyclization in DMSO-d_6 in the dark and exists as mixtures with **1a**:**1b** ~ 1:4 at the dark equilibrium.

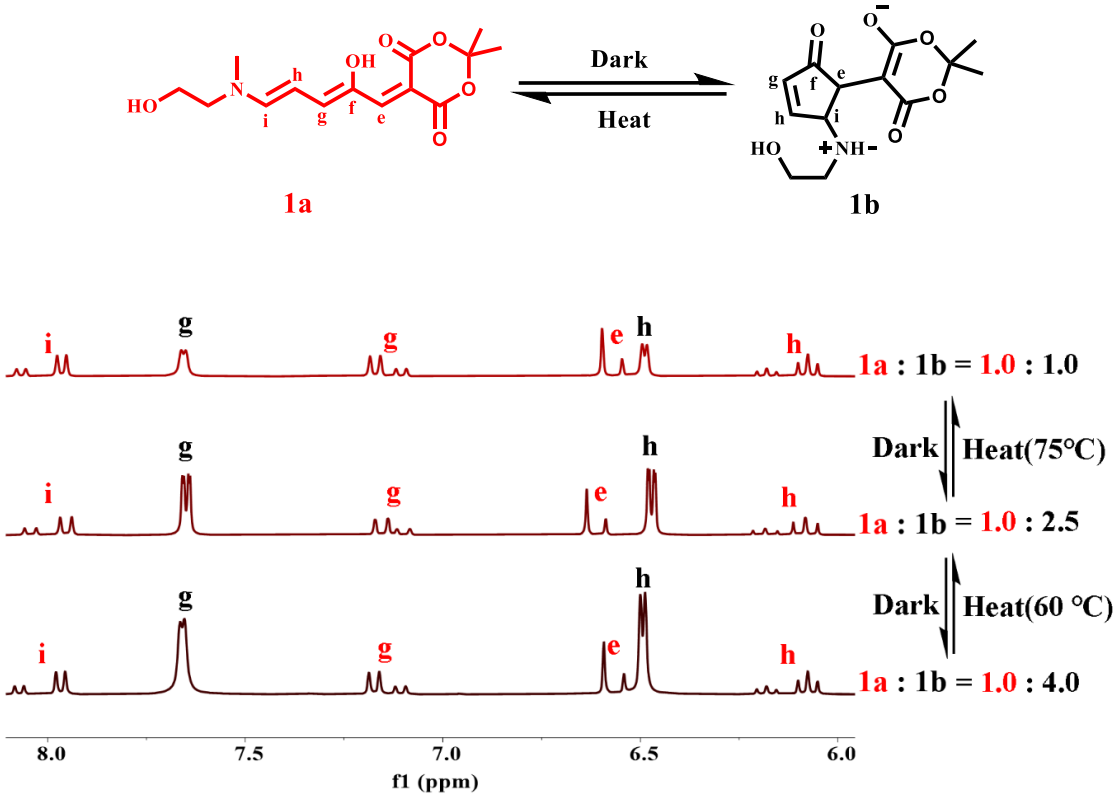

Figure S6. Stacked ^{1}H NMR spectra (500 MHz, DMSO-d_6) and heating show a shift of **1a**/**1b** ratio at different temperatures in the dark. The spectrum at 25 °C was measured after dark equilibrium (three days of resting), while the other two spectra at 60 and 75 °C were measured immediately at 25 °C after heating for 5 minutes.

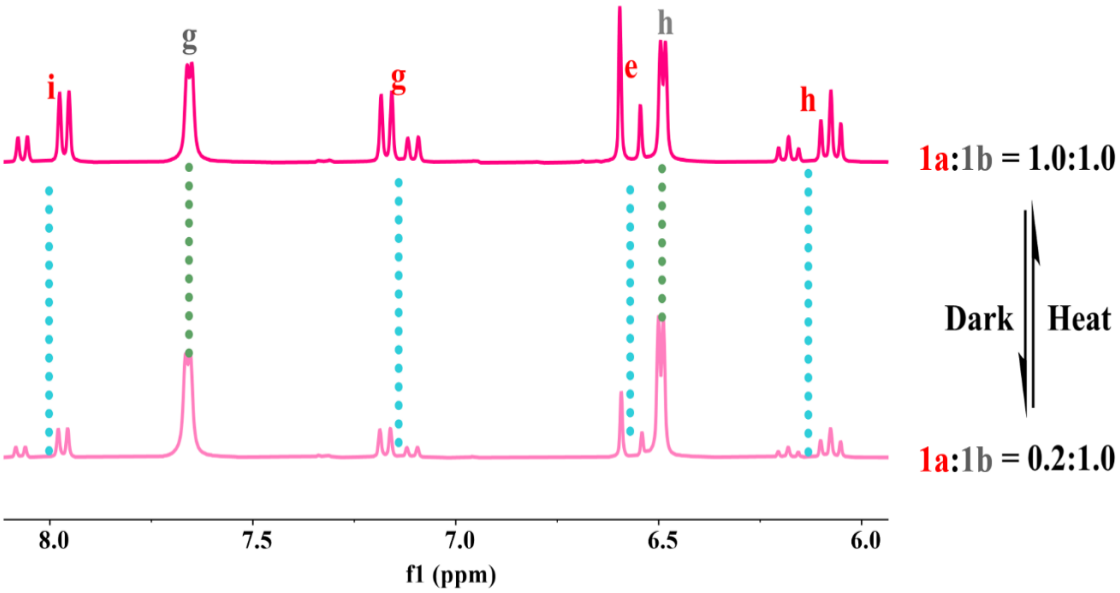

Figure S7. Stacked ^{1}H NMR spectra (500 MHz, DMSO-d_6) indicate the reversible thermal driven **1a↔1b** switching. The spectrum below was measured after dark equilibrium at 25 °C (three days of resting), and the spectrum above was measured immediately after heating at 75 °C for 5 minutes.

4. Acidity-driven isomerization

4.1 Method of obtaining 1c

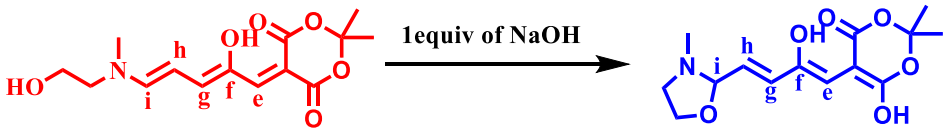

1a **1c**

1c: 1 equivalent of NaOH (dissolved in methanol) were added to the DMSO solution of **1c**, resulting in the formation of a light yellow solution of **1c**.

1c: ^{1}H NMR (500 MHz, DMSO-d_6) δ 5.96 (d, J = 15.0 Hz, 1H), 5.31 – 5.27 (m, 1H), 5.16 (s, 1H), 4.02 (d, J = 7.5 Hz, 1H), 3.74 (dt, J = 8.7, 4.3 Hz, 2H), 3.14 – 3.2 (m, 1H), 2.44 (m, 1H), 2.16 (s, 1H), 1.49 (s, 6H).

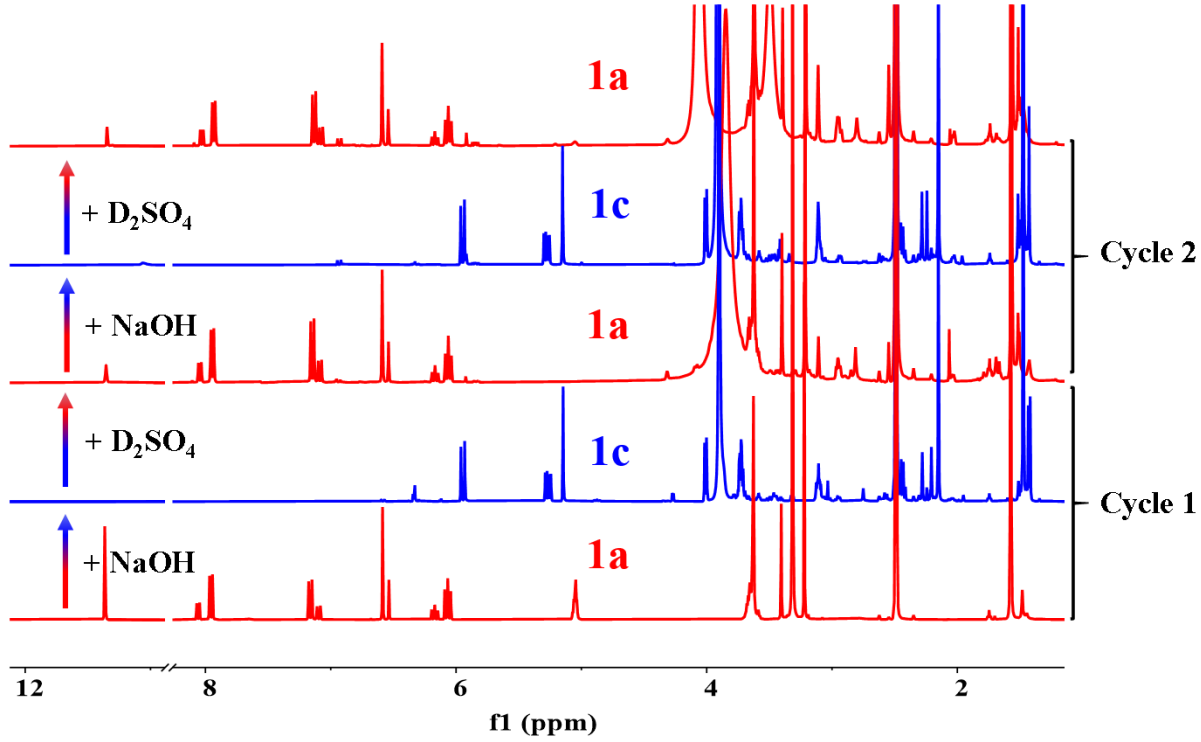

Figure S8. Stacked ^{1}H NMR spectra (500 MHz, DMSO-d_6, room temperature) in the entire region show the reversible transformation between **1a** and **1c** upon an alternative base (1 equiv of NaOH) and acid (0.5 equiv of D_2SO_4) titrations.

4.2 Concentration dependence

A quantitative conversion from **1a** to **1c** relies on a proper concentration. At low concentrations (~10 μM), alkalization-induced color bleaching is inadequate (Figure S9), indicating that **1c** is not stable in such an environment.

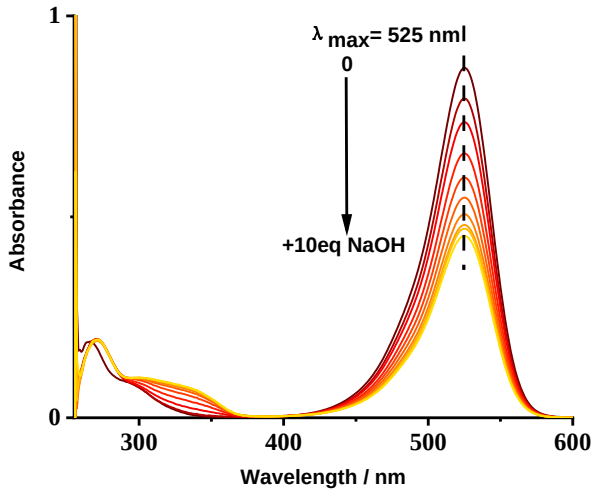

Figure S9. Alkalization-induced color bleaching of **1a** is inadequate at low concentrations (in DMSO, ~10 uM), where NaOH was prepared in MeOH (1 mM), indicating a strong concentration dependence of the stability of **1c**.

4.3 Spontaneous conversion from 1c to 2

We noticed a spontaneous conversion from **1c** to **2** during the acquisition of NMR spectra. The addition of external water can accelerate the transformation from **1c** to **2**.

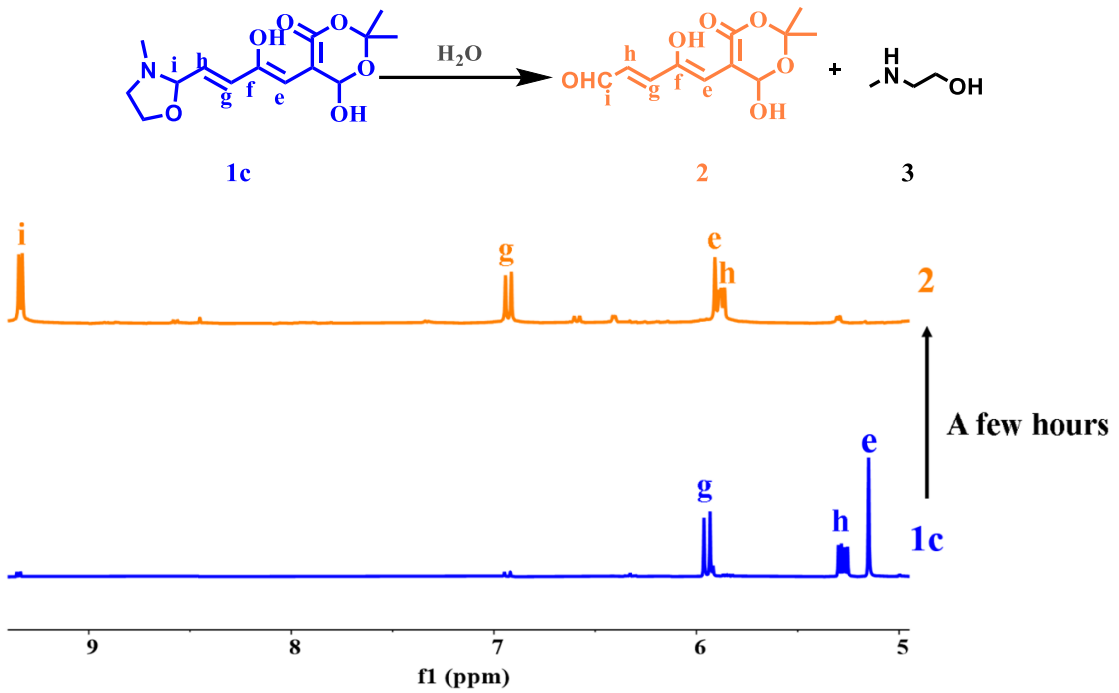

Figure S10. Comparison of ^{1}H NMR spectra before (bottom) and after (top) HSQC NMR spectrum acquisition of **1c** in DMSO-d_6, indicating a spontaneous conversion from **1c** to **2**+**3**.

4.4 The direct acquisition method of 2

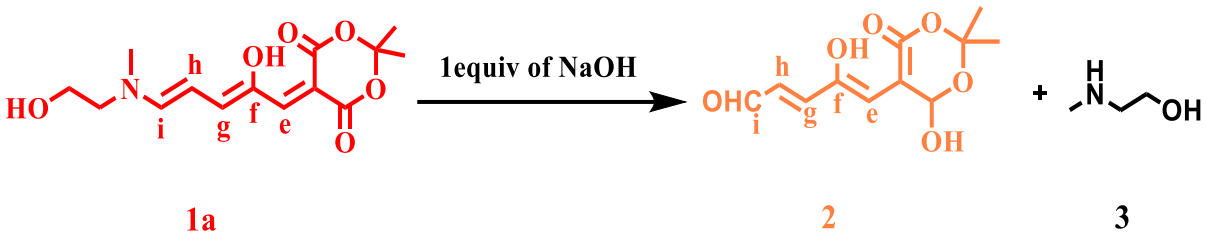

2: 1 equivalent of NaOH (dissolved in deionized water) was added to the DMSO solution of **1a**, forming a dark yellow solution of **2**. ^{1}H NMR (500 MHz, DMSO-d_6) δ 9.29 (d, J = 8.7 Hz, 1H), 7.01 (d, J = 14.4 Hz, 1H), 5.91 (dd, J = 14.3, 8.6 Hz, 1H), 5.81 (s, 1H), 3.42 (t, J = 5.8 Hz, 2H), 2.45 (t, J = 5.8 Hz, 2H), 2.19 (s, 3H), 1.51 (s, 6H).^{13}C{^{1}H} NMR (125 MHz, DMSO-d_6) δ 194.22, 166.55, 120.94, 117.34, 102.15, 80.25, 67.86, 60.35, 53.83, 36.10, 26.31. HRMS (ESI+) calc. for $C_{11}H_{12}O_6$ [**2**]$^{+\cdot}$: 240.0637, found: 240.0871.

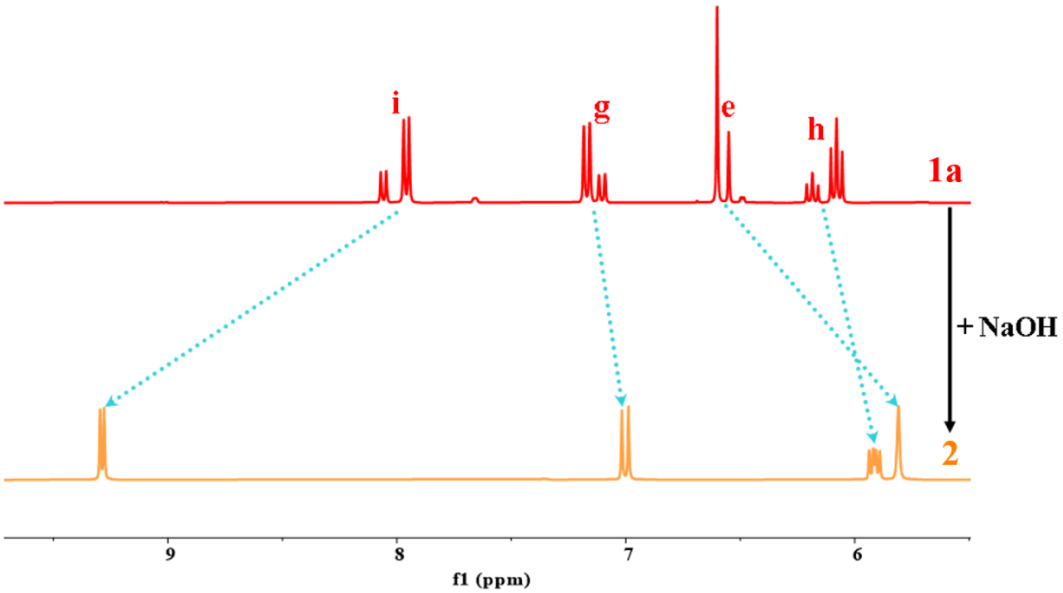

Figure S11. Stacked ^{1}H NMR spectra (500 MHz, DMSO-d_6, room temperature) show the conversion from **1a** to **2+3** upon the addition of 1 equiv of NaOH in D_2O (1 M).

4.5 Structural assignment for 2:

For the following reasons, **2** was assigned to the dienal structure. 1) The lack of NOE effects between Hi and the methyl and methylene groups in **2** (Figure S38and the following scheme), in contrast to the apparent presence of NOE effects in **1a** (Figure S24), implying that the C-N bond is broken and the sample decomposes. 2) The presence of aldehyde groups in the decomposition product is indicated by the ^{1}H signal at 9.29 ppm (Figure S34) and the ^{13}C signal at 193 ppm (Figure S35). 3) The upfield signals agree perfectly with the raw amine (Figure S13), confirming the breakage of the C-N bond and that the product was a 1:1 mixture of raw amine and dienal. 4) High-resolution mass spectrum was applied (Figure S46), and the m/z 240.0871 peak corresponds to the decomposed aldehyde $M^{+\cdot}$ and m/z 222.0764 for the (M-18) peak, confirming the presence of the dienal product. 5) The presence of aldehyde can be determined using Tollens tests.

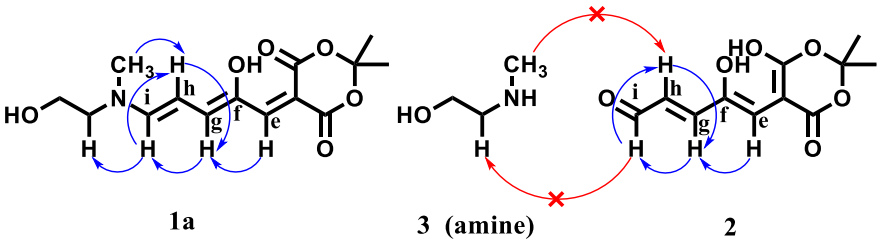

The above schemes show the prominent NOE correlation in the nuclear Overhauser effect correlation spectra (NOESY) of **1a** and **2**.

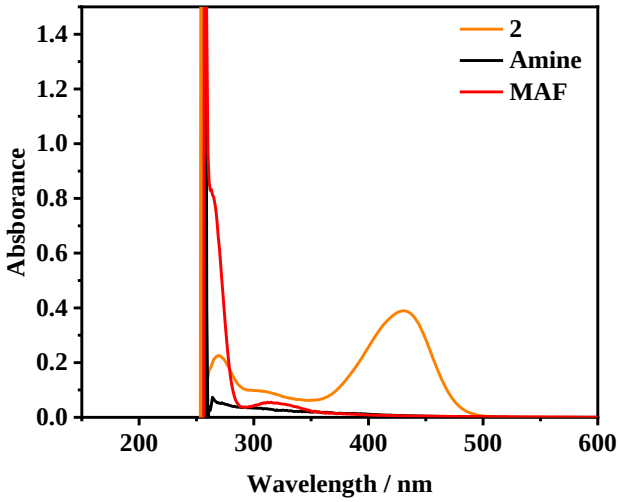

Figure S12. The UV-Vis absorption spectra of **2**, raw amine, and MAF show that **2** is different from the raw materials.

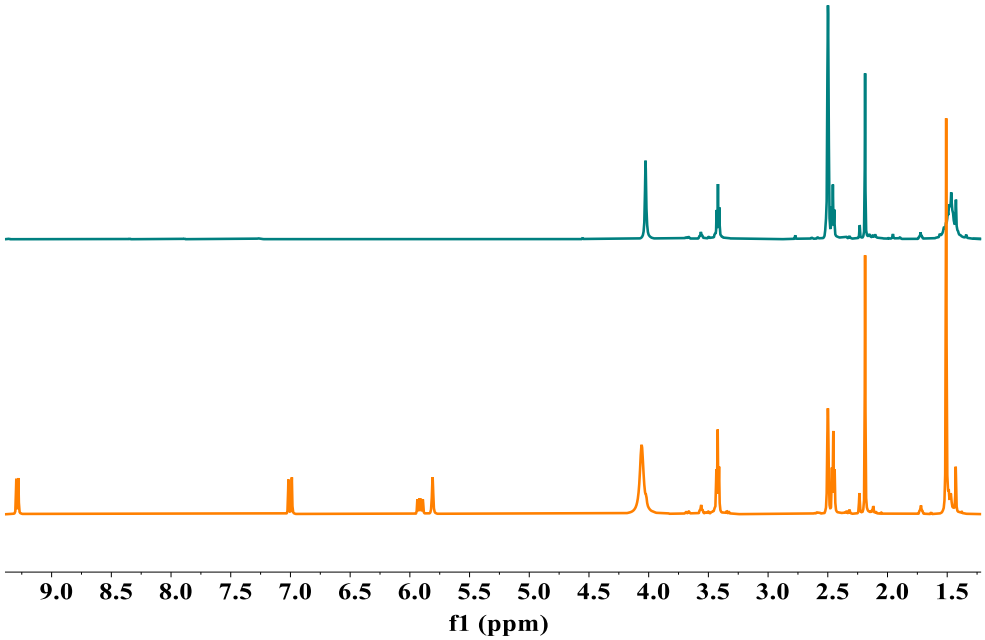

Figure S13. Stacked ^{1}H NMR (500 MHz, DMSO-d_6, 298 K) spectra of **2** before (bottom) and after (top) exposure to light, indicating that **2** tends to undergo retro-reaction upon light irradiation.

4.6 structural transitions: 1a↔1c→2+3→(1a) →1b

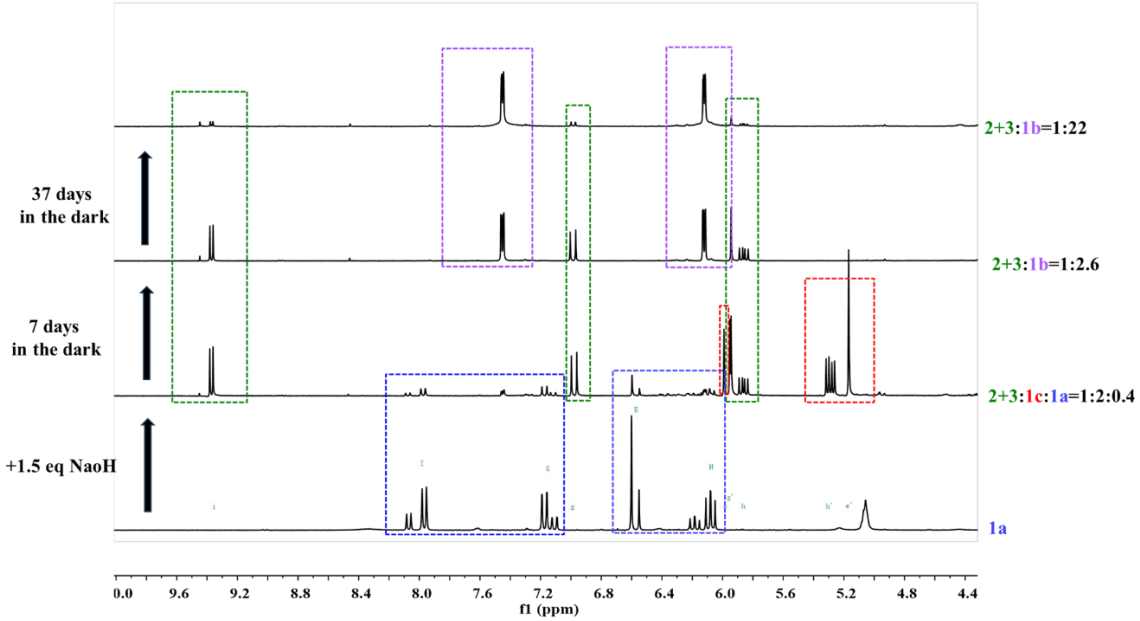

Figure S14. The time evolution data of ^{1}H NMR (500 MHz, DMSO-d_6, 298 K) signals clearly support the gradual accumulation of **1b** over time.

4.7 Condensation of 2 and 3 to reestablish 1a

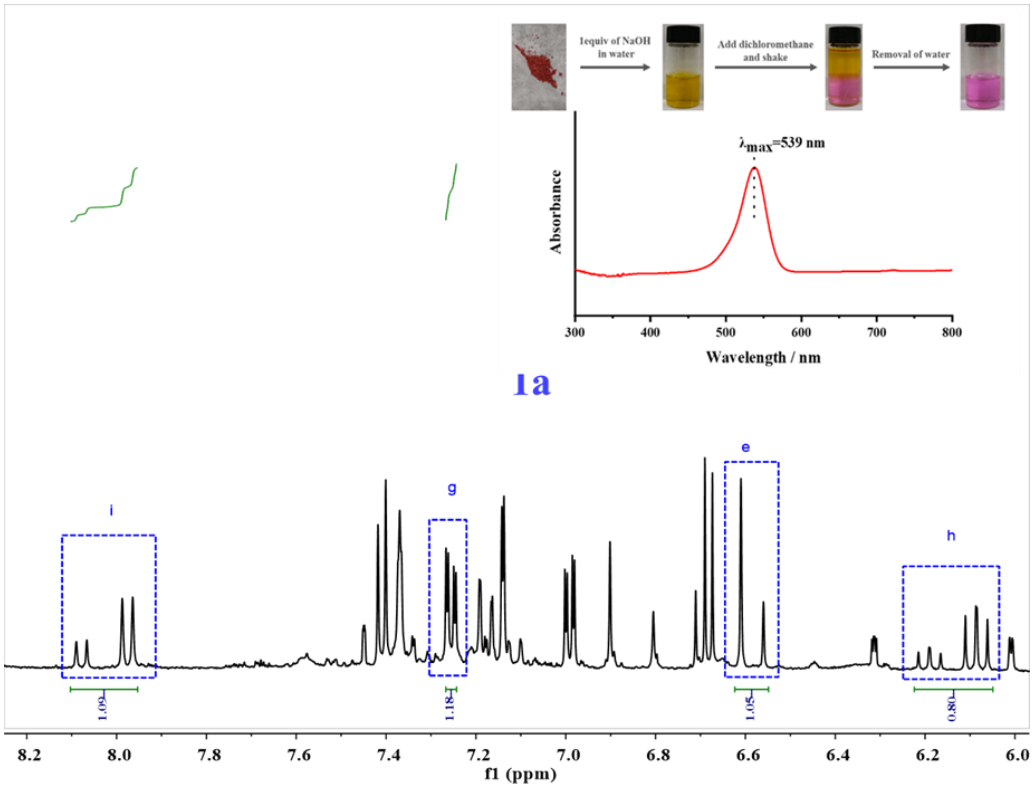

Figure S15. Dichloromethane extraction of hydrolysis products (**2**+**3**) in an aqueous solution can drive a direct recovery to **1a**, as evidenced by an immediate reappearance of its characteristic absorption in NMR and UV-Vis.

5. Reversible thermochromism

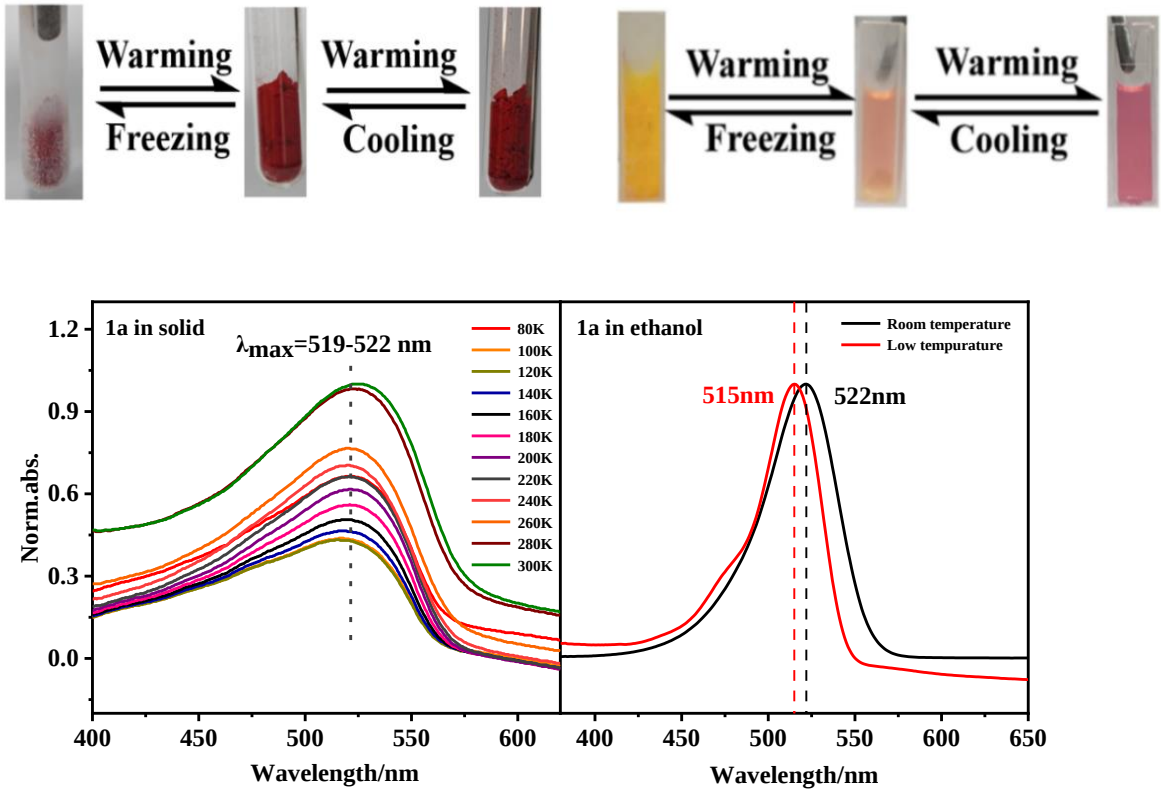

Figure S16. The photographs (top) depict the distinct color responses of **1a** in both solid and ethanol solution to temperature changes. The corresponding UV-Vis absorption spectra (bottom) provide further evidence for the observed color changes as determined visually. When exposed to various temperatures, the solid sample shows minimal alterations in the absorption band, even when cooled to 80 K. Monitoring temperature-dependent changes in the solution state is challenging due to the aggregation caused by cooling. Nevertheless, we observed a blueshift phenomenon upon cooling, although the precise temperature remains unknown. (The solution at low temperature was tested after gradually melting following removal from liquid nitrogen.)

Table S2. Thermochromism of **1a** in different solvents.

	MeOH	MeCN	DMSO	Toluene
298K				
77K				
77K (UV)				

Table S3. Comparison of the thermochromism of isomer **1a**, **DASA-1**[6], **DASA-2**[6] **DASA-3**[6], and **DASA-4**[6] in methanol. The difference in their color changes is possibly related to the degree of charge separation in their open forms.

Several so-called first and third-generation DASAs (DASA-1, DASA-2), which tend to have a higher zwitterionic resonance of the open form[6] all show obvious thermochromism. A second-generation derivative (DASA-3) with less charge-separation[6], DASA-4 with a different dipolar nature, and **2** with a highly zwitterionic nature are less prone to undergo thermochromism.

	1a	**DASA-1**	**DASA-2**	**DASA-3**	**DASA-4**
	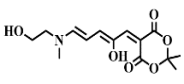	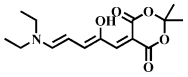	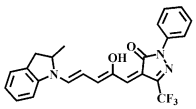	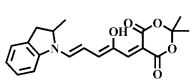	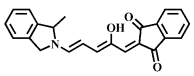
298 K					
77 K					

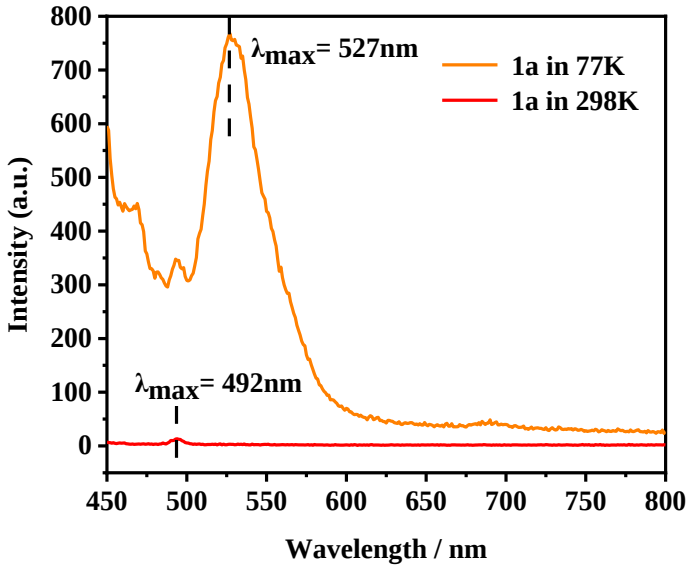

Figure S17. Fluorescence emission spectra of **1a** (in DMSO, 10^{-2} μM) at 298K and 77K (excitation wavelength = 430 nm), showing the significant enhancement of fluorescence at low temperatures.

6. FTIR spectroscopy

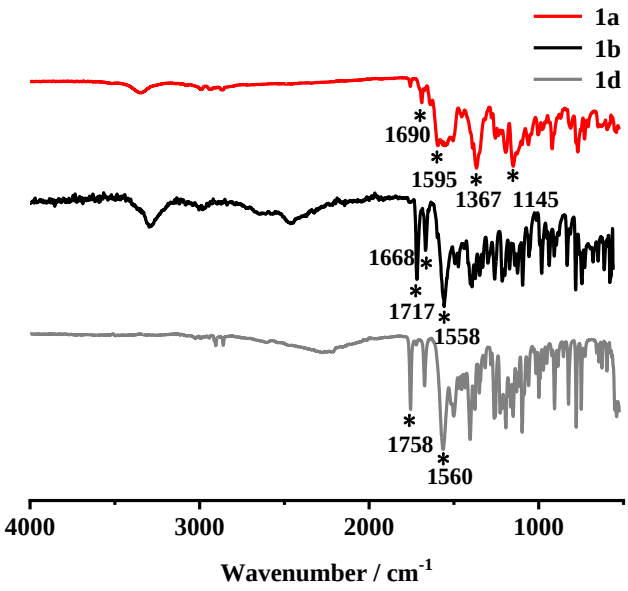

Figure S18. FTIR spectra of **1a** (in red), **1b** (in black), **1d** (in grey) in the region of 4000 – 500 cm^{-1} at room temperature. For **1a**, the peak at 1690 cm^{-1} is attributed to the stretching vibration of C=O, the peak at 1595 cm^{-1} is attributed to the stretching vibration of -C=C-C=C- groups, 1367 (C-O and C-H deformation bands), and 1145 cm^{-1} (C-O stretching band) clearly identify the triene-enol part. For **1b**, the peaks at 1717 and 1558 cm^{-1} are attributed to the stretching vibration of C=O on the five and six-membered rings, respectively. The peak at 1668 cm^{-1} is attributed to the stretching vibration of -C=C- on the five and six-membered rings. For **1d**, the peaks at 1758 and 1560 cm^{-1} are attributed to the stretching vibration of C=O on the five and six-membered rings, respectively[9, 10].

7. NMR spectra

7.1 ^{1}H NMR spectrum of 1a in DMSO-d_6

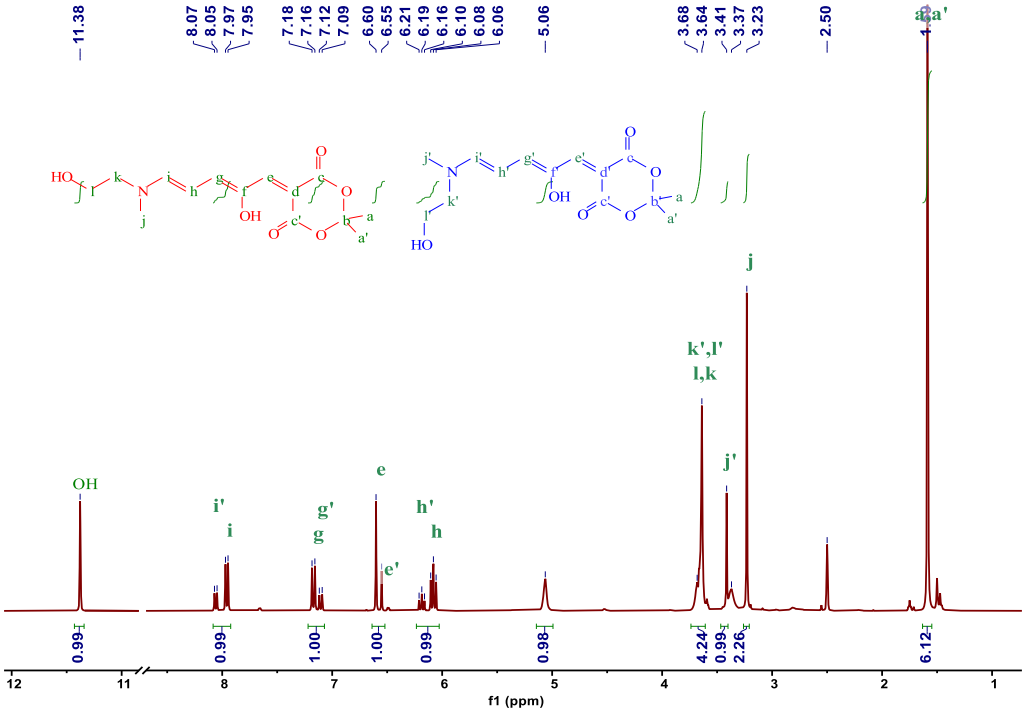

Figure S19. ^{1}H NMR spectrum of **1a** in DMSO-d_6 (freshly dissolved, 500 MHz, room temperature). Two sets of signals with a ratio ~1:3 were observed and were attributed to the trapping of stereoisomers. The major linear isomer was tentatively assigned given less steric hindrance, i.e., with the smallest group oriented perpendicular to the triene chain[4].

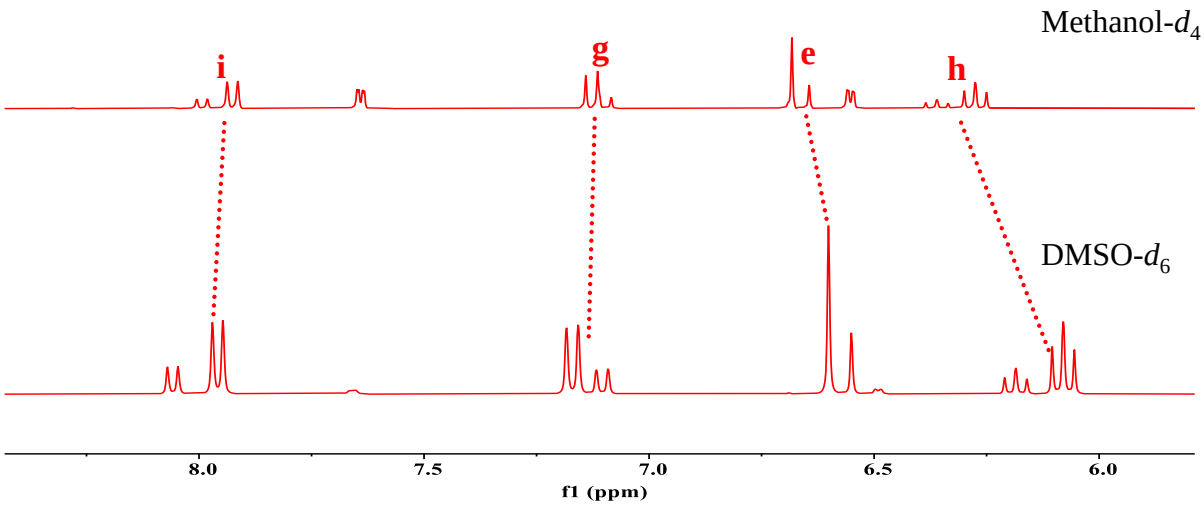

Figure S20. Stacked ^{1}H NMR spectra of **1a** in DMSO-d_6 and methanol-d_4 (freshly dissolved, 500 MHz, room temperature).

7.2 $^{13}C\{^{1}H\}$ NMR spectrum of 1a in DMSO-d_6

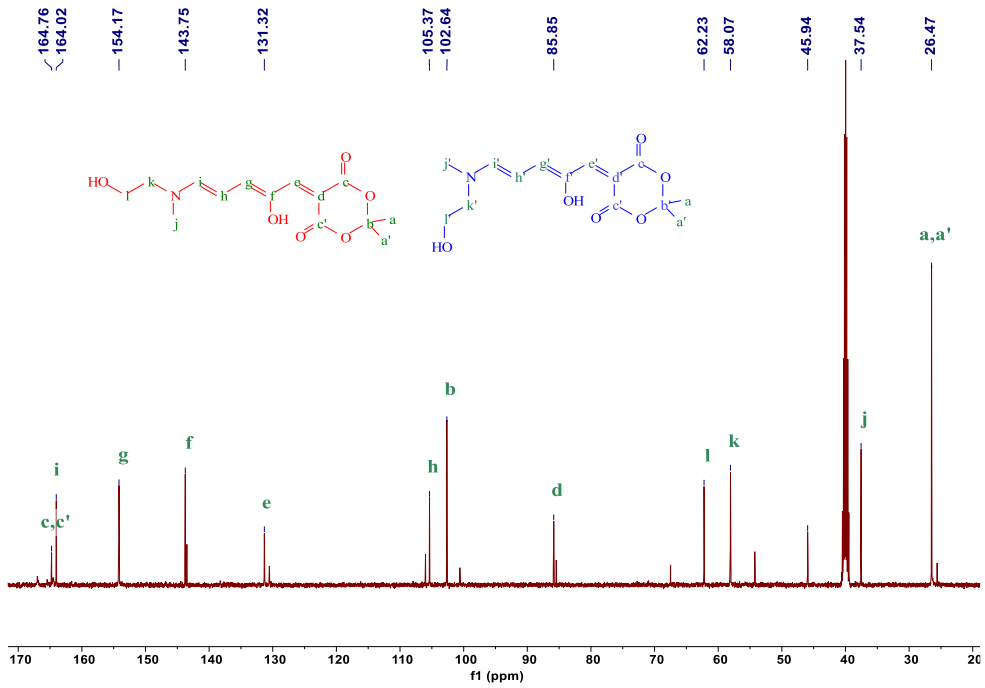

Figure S21. $^{13}C\{^{1}H\}$ NMR spectrum of **1a** in DMSO-d_6 (125 MHz, room temperature).

7.3 ^{1}H, ^{1}H–COSY NMR spectrum of 1a in DMSO-d_6

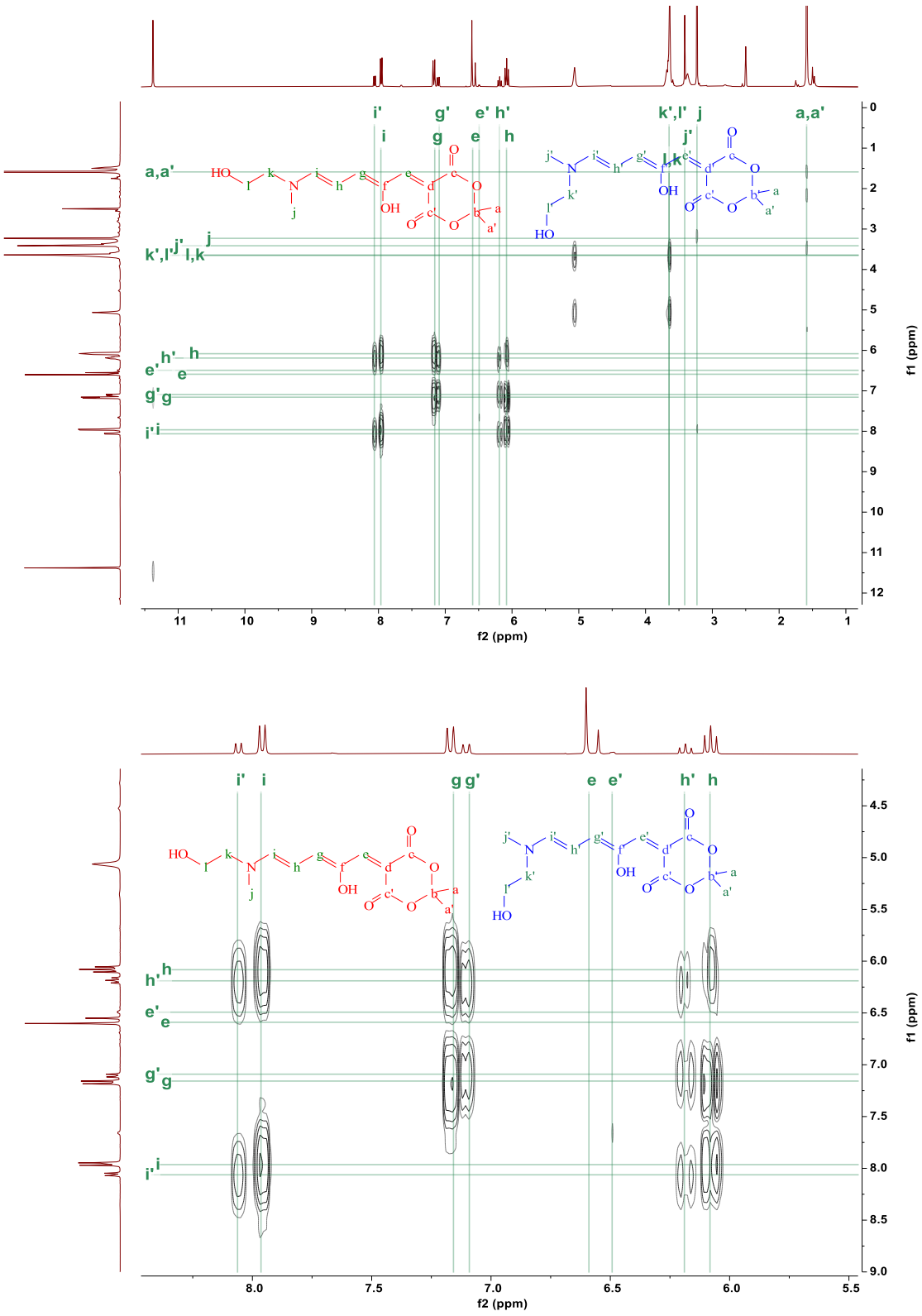

Figure S22. Entire (top) and zoomed (bottom) ^{1}H, ^{1}H–COSY NMR spectra of **1a** in DMSO-d_6 (500 MHz, room temperature). The major linear isomer was tentatively assigned in view of less steric hindrance, i.e. with the smallest group oriented perpendicular to the triene chain[4].

7.4 HSQC NMR spectrum of 1a in DMSO-d_6

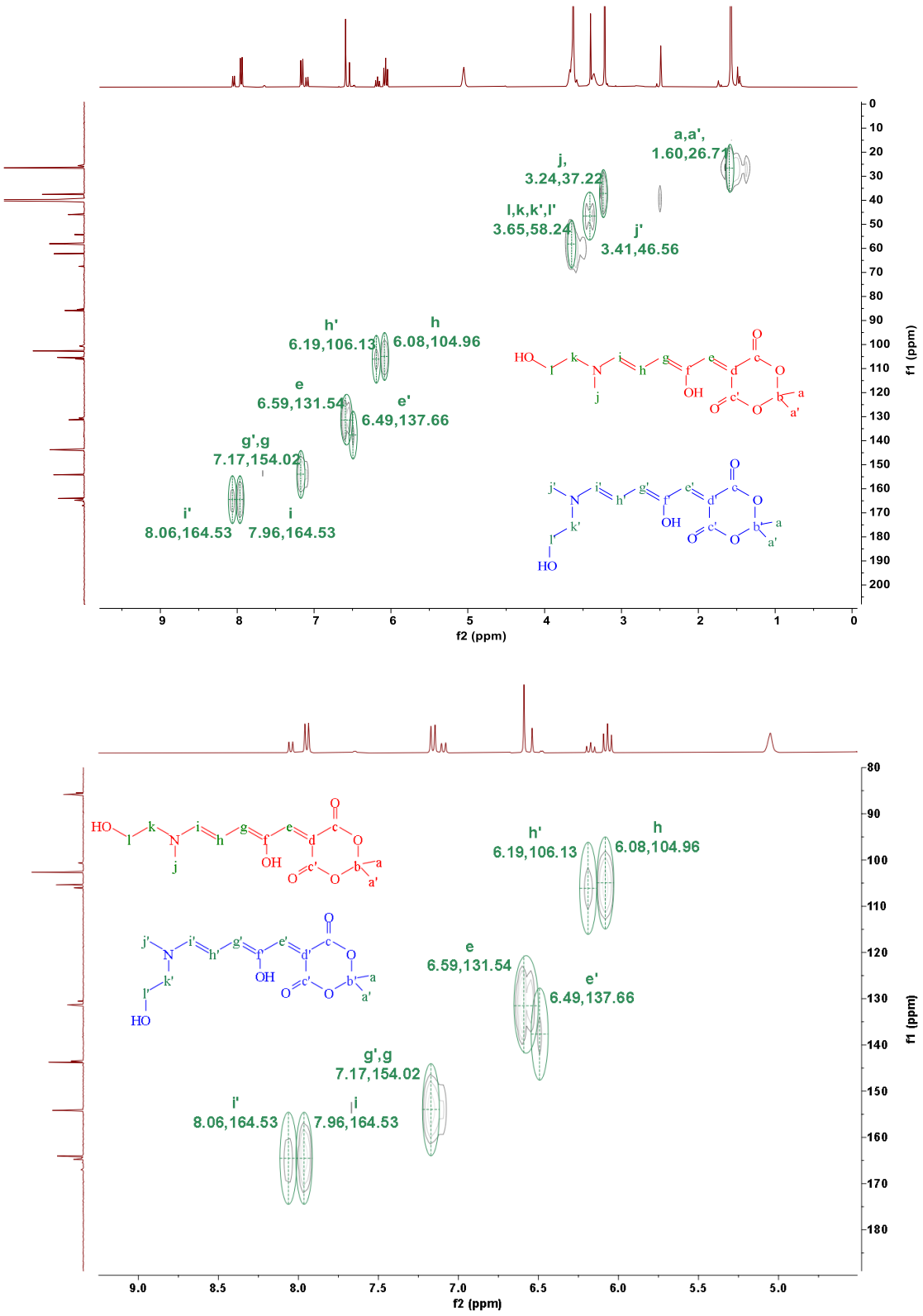

Figure S23. Entire (top) and zoomed(bottom) HSQC NMR spectra of **1a** in DMSO-d_6 (freshly dissolved, 500 MHz, room temperature).

7.5 NOESY NMR spectrum of 1a in DMSO-d_6

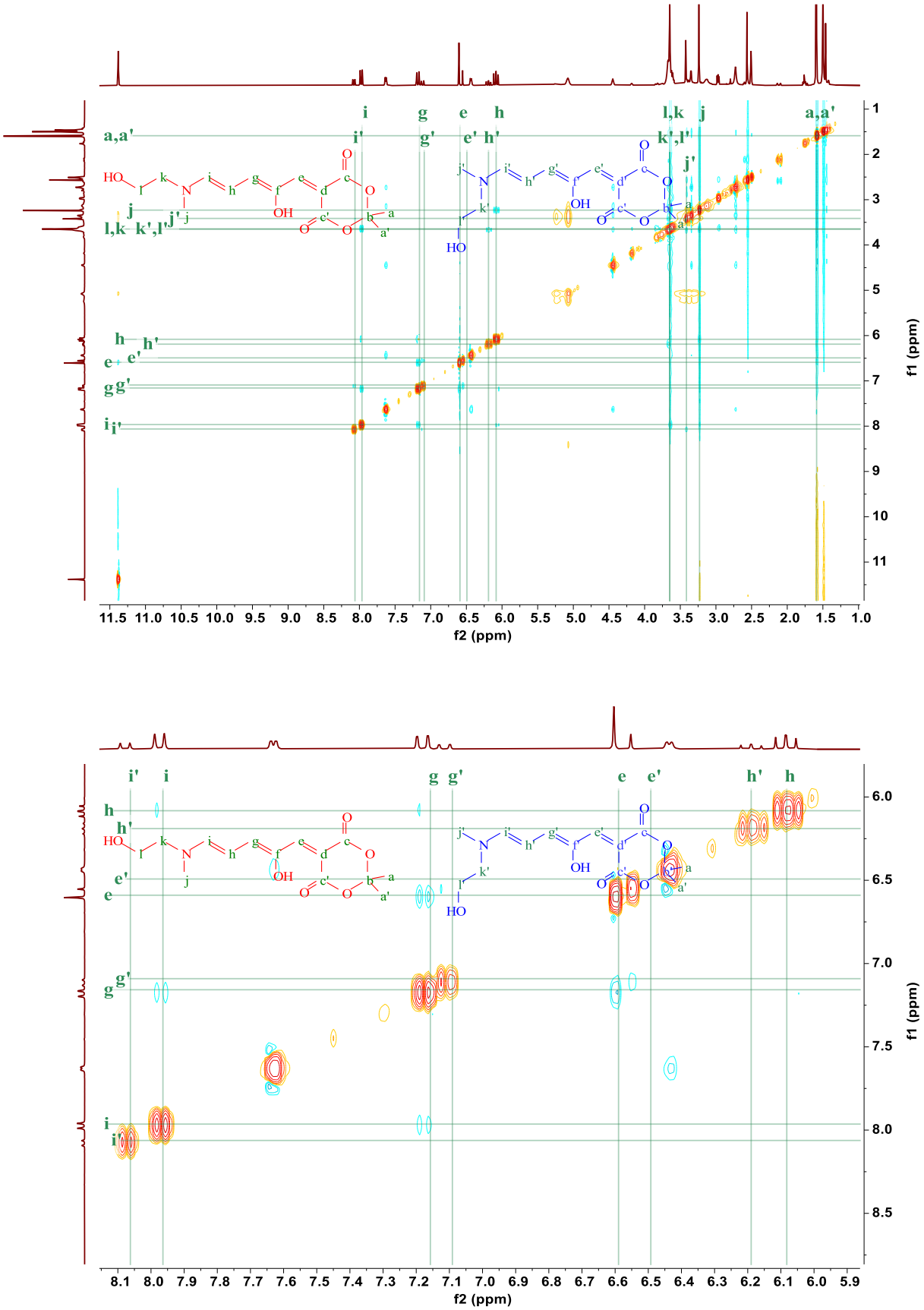

Figure S24. Entire (top) and zoomed (bottom) NOESY NMR spectra of **1a** in DMSO-d_6 (400 MHz, room temperature).

7.6 ^{1}H NMR spectrum of 1b in D_2O

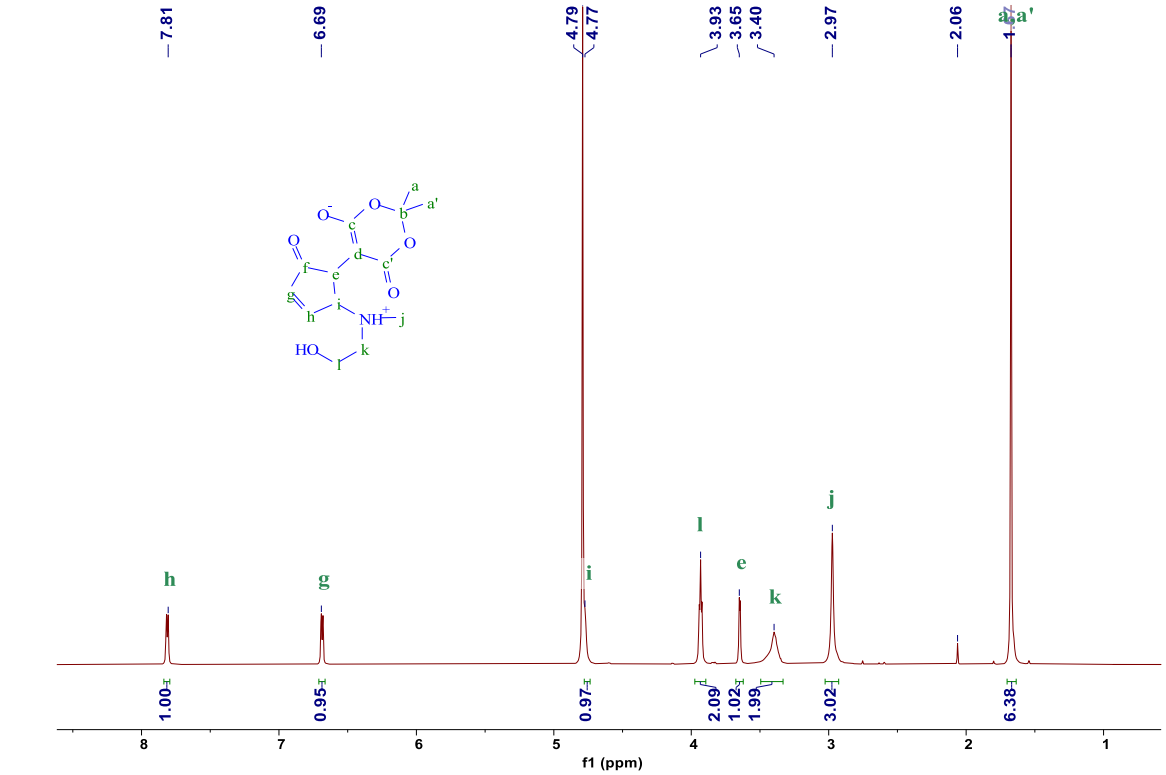

Figures S25. ^{1}H NMR spectrum of **1b** in D_2O (500 MHz, room temperature).

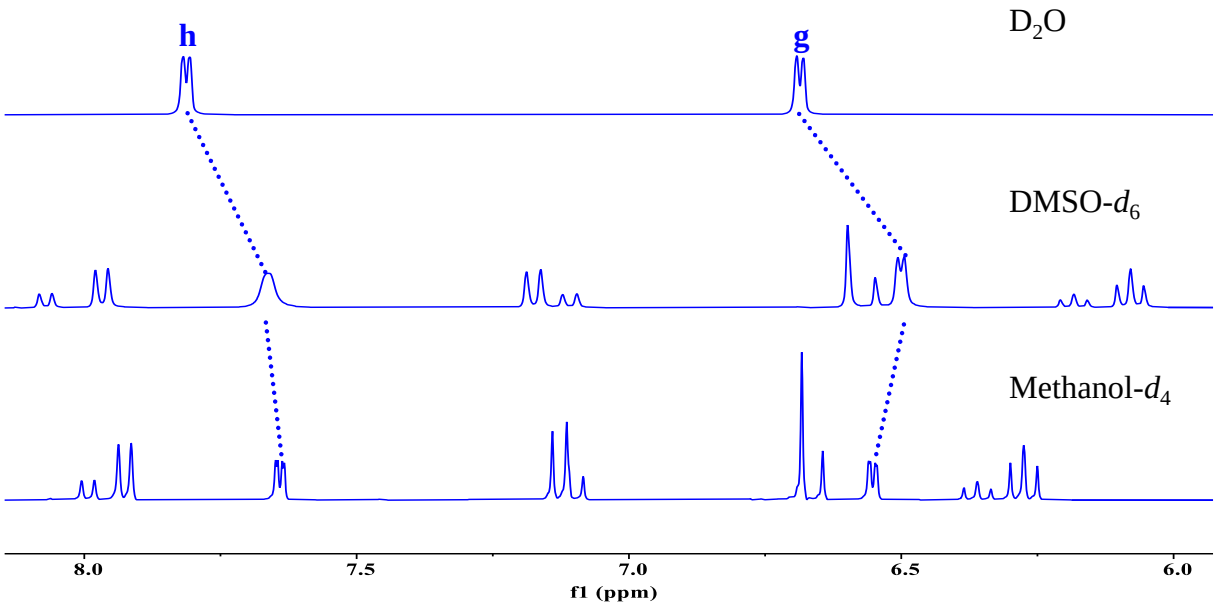

Figure S26. Stacked ^{1}H NMR spectra of **1b** in D_2O, DMSO-d_6 and methanol-d_4 (freshly dissolved, 500 MHz, room temperature). It should be noted that it is a mixture of **1a** and **1b** in DMSO-d_6 and methanol-d_4, whereas we were only seeking to compare the ^{1}H NMR spectra of **1b** in different solvents.

7.7 $^{13}C\{^{1}H\}$ NMR spectrum of 1b in D_2O

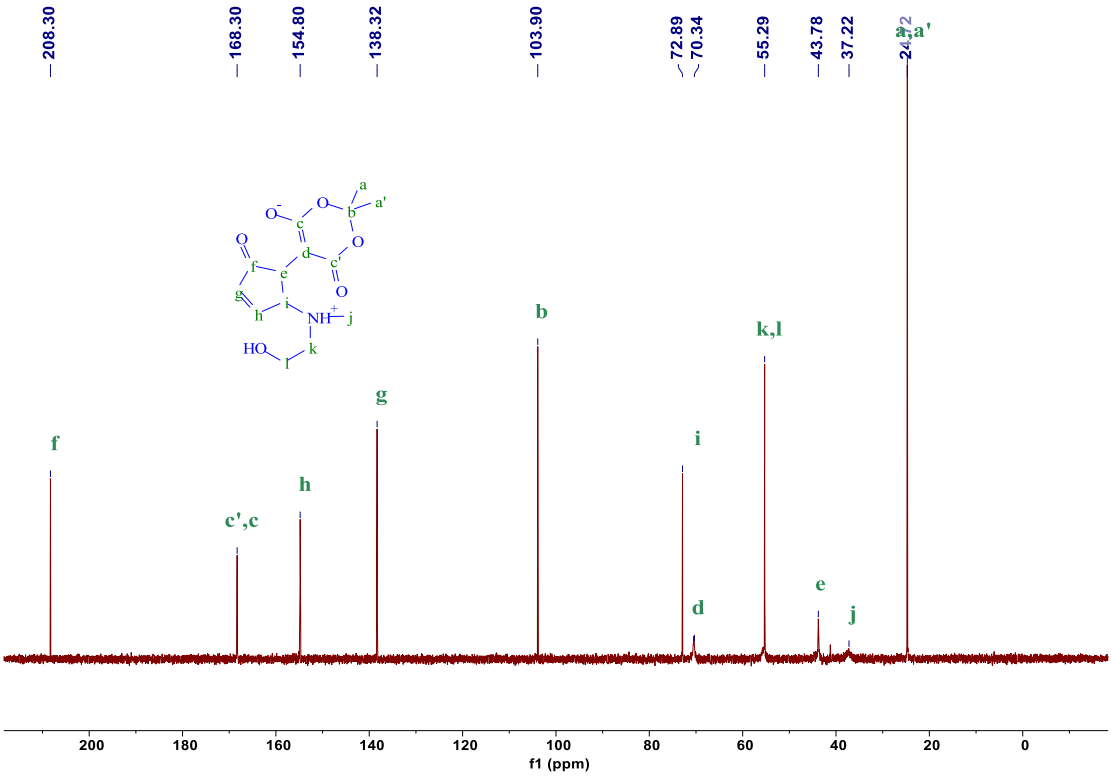

Figure S27. $^{13}C\{^{1}H\}$ NMR spectrum of **1b** in D_2O (125 MHz, room temperature).

7.8 ^{1}H, ^{1}H–COSY NMR spectrum of 1b in D_2O

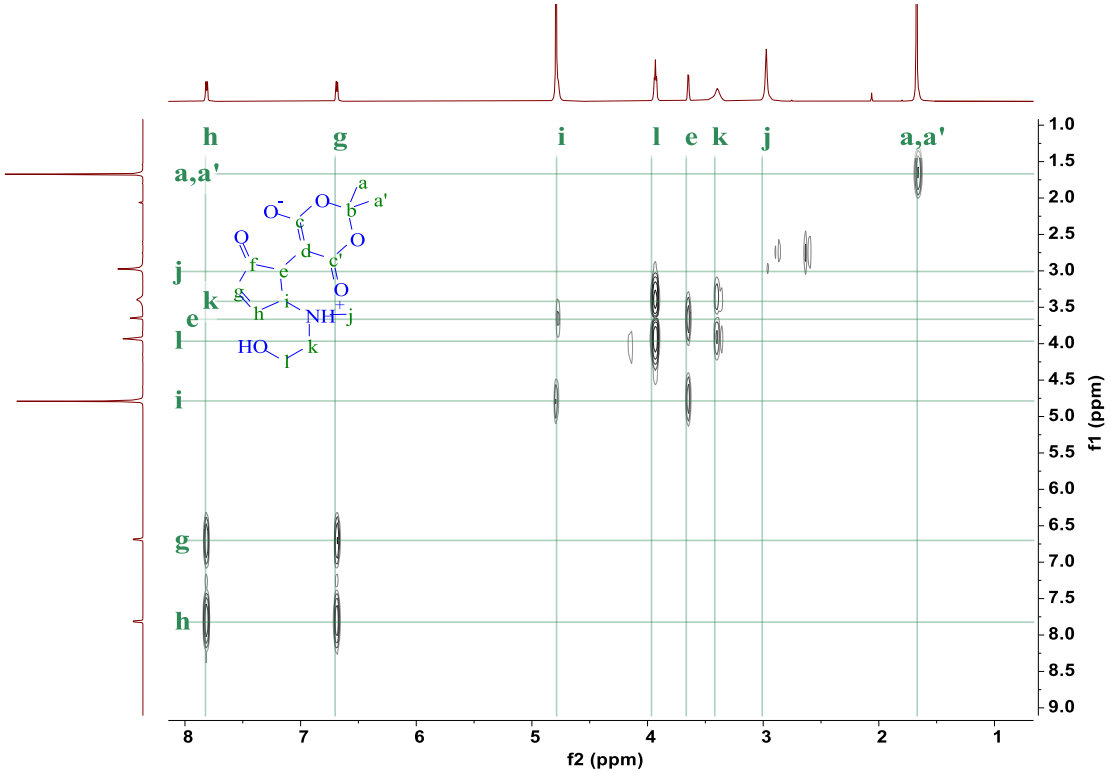

Figure S28. ^{1}H, ^{1}H-COSY NMR spectrum of **1b** in D_2O (500 MHz, room temperature).

7.9 HSQC NMR spectrum of 1b in D_2O

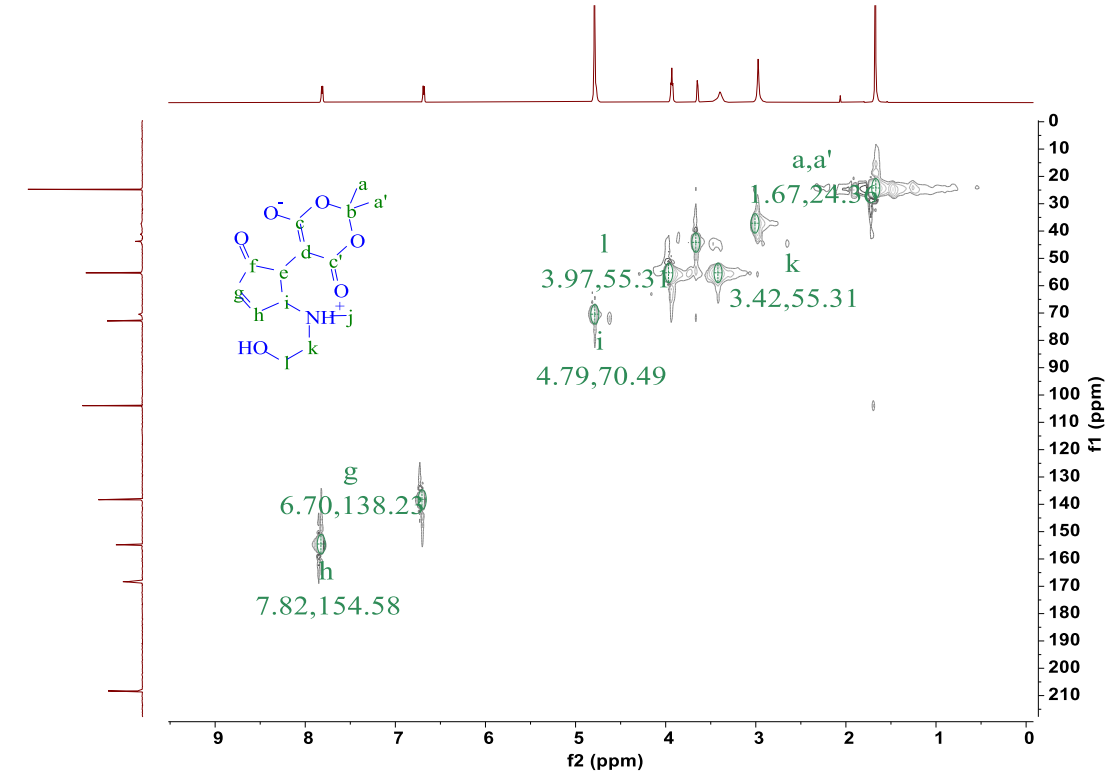

Figure S29. HSQC spectrum of **1b** in D_2O (500 MHz, room temperature).

7.10 ^{1}H NMR spectrum of 1c in DMSO-d_6

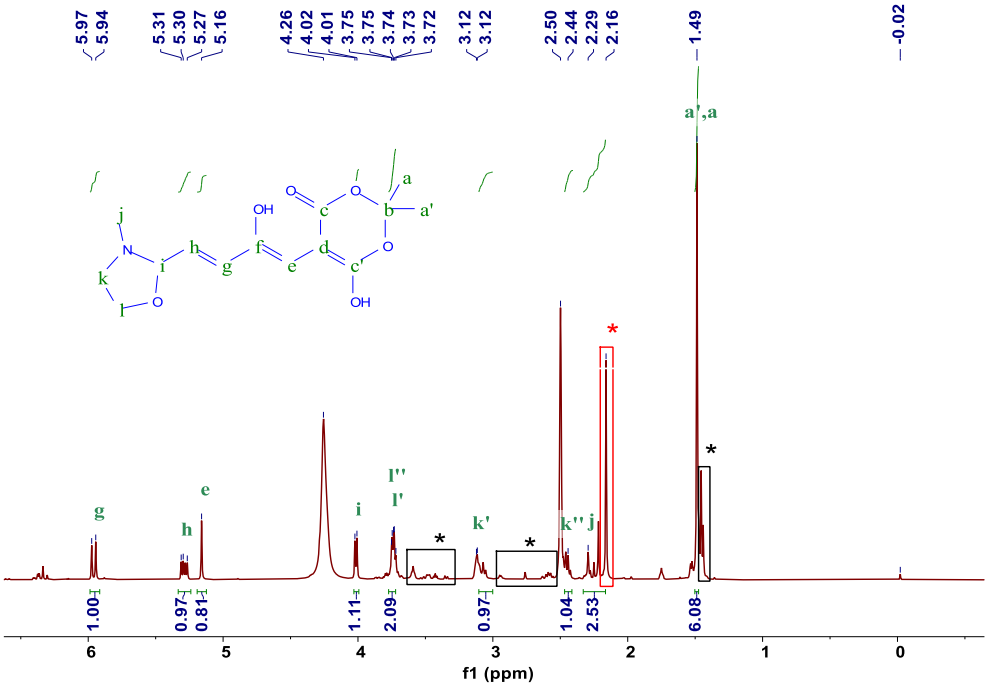

Figure S30. ^{1}H NMR spectrum of **1c** (500 MHz, room temperature), obtained by the addition of 1 equiv of NaOH (dissolved in a minimum amount of methanol-d_4) to the DMSO-d_6 solution of **1a**. Impurities in the spectrum due to the formation of **2** and **3** are marked with a black * and red *, repspectively.

7.11 ^{13}C{^{1}H} NMR spectrum of 1c in DMSO-d_6

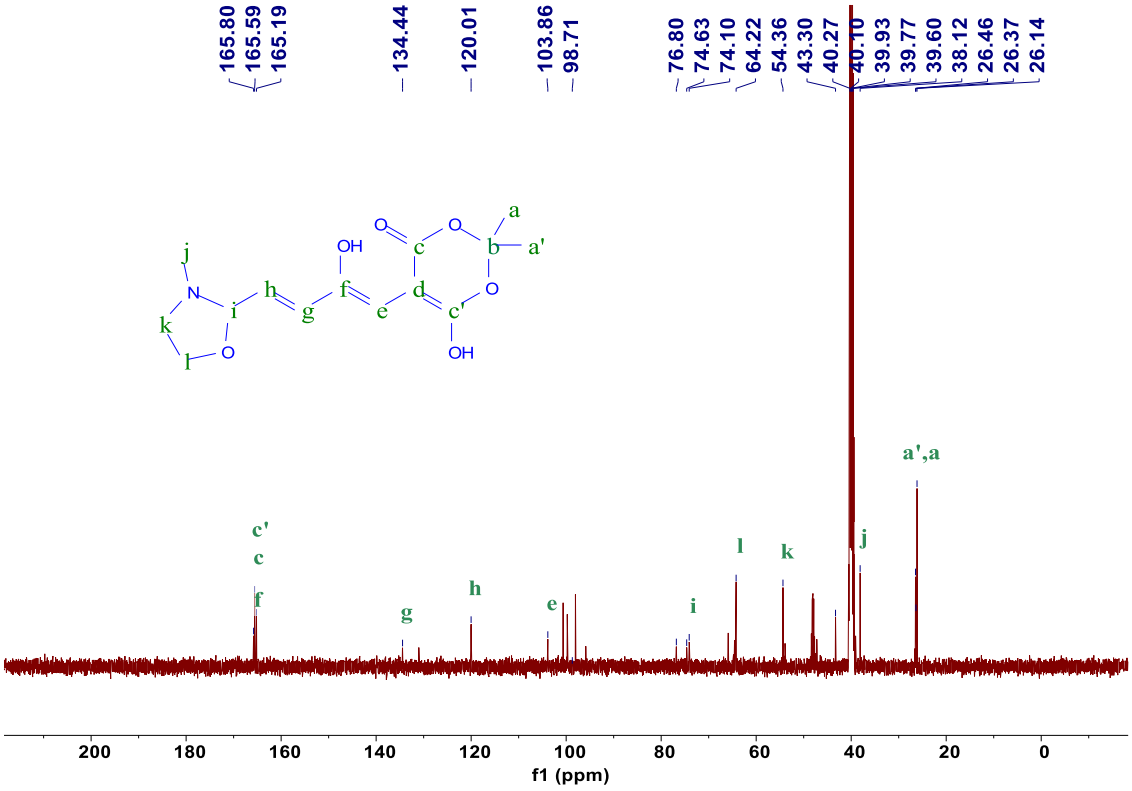

Figure S31. ^{13}C{^{1}H} NMR spectrum of **1c** (125 MHz, room temperature), obtained by the addition of 1 equiv of NaOH (dissolved in a minimum amount of methanol-d_4) to the DMSO-d_6 solution of **1a**. It should be noted that there is a spontaneous conversion from **1c** to **2** during spectra acquisition, which gives rise to the complexity of the spectra.

7.12 ^{1}H, ^{1}H–COSY NMR spectrum of 1c in DMSO-d_6

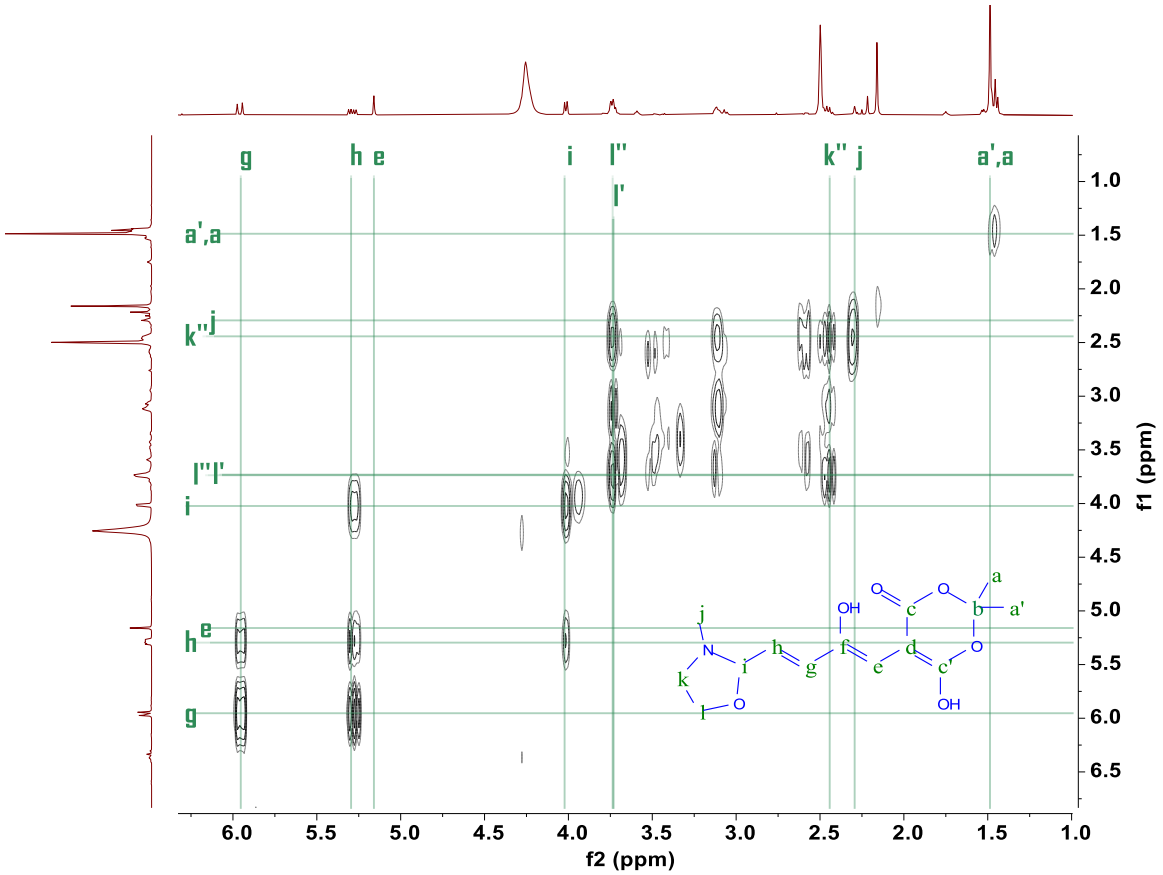

Figure S32. ^{1}H, ^{1}H-COSY NMR spectrum of **1c** (500 MHz, room temperature), obtained by the addition of 1 equiv of NaOH (dissolved in a minimum amount of methanol-d_4) to the DMSO-d_6 solution of **1a**.

7.13 HSQC NMR spectrum of 1c in DMSO-d_6

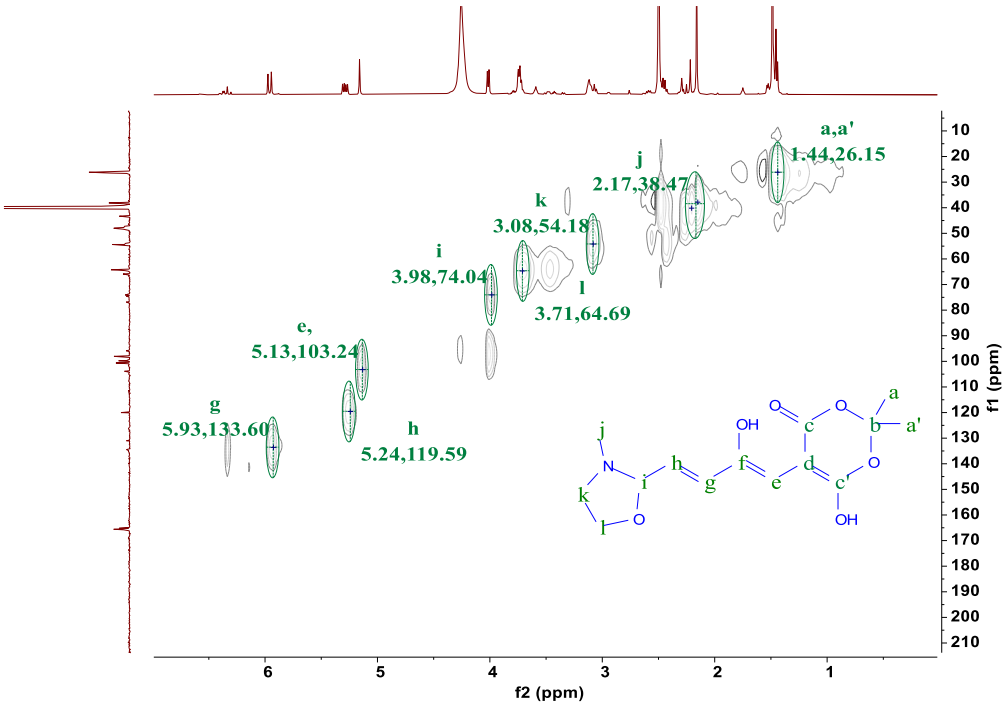

Figure S33. HSQC spectrum of **1c** (500 MHz, room temperature), obtained by the addition of 1 equiv of NaOH (dissolved in a minimum amount of methanol-d_4) to the DMSO-d_6 solution of **1a**. It should be noted that there is a spontaneous conversion from **1c** to **2** during spectra acquisition, which gives rise to the complexity of the spectra.

7.14 ^{1}H NMR spectrum of 2 in DMSO-d_6

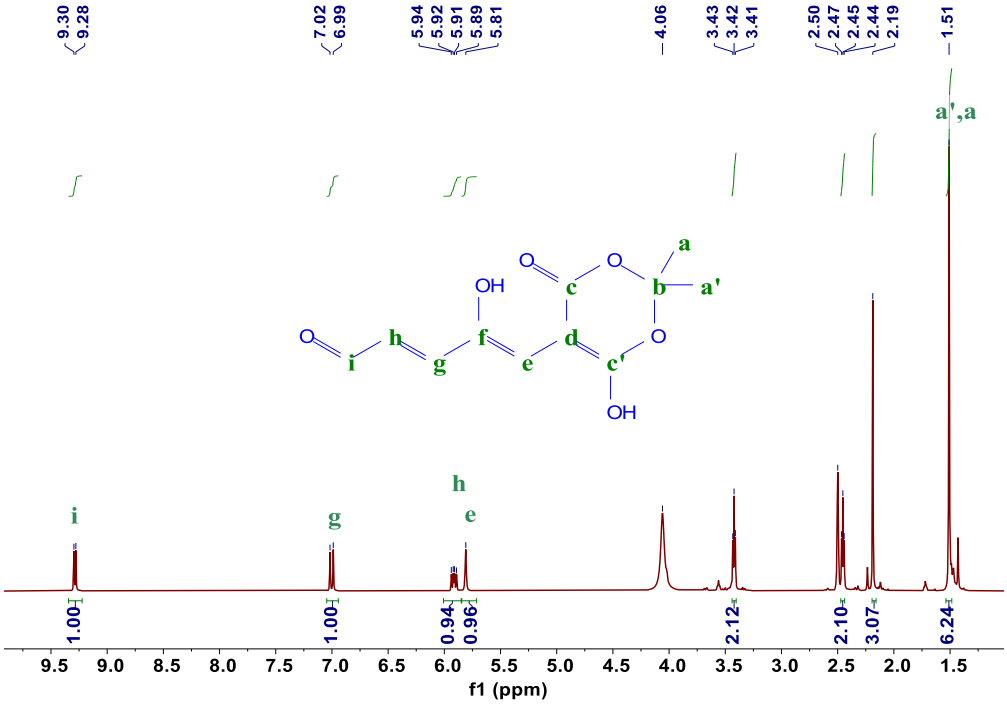

Figure S34. ^{1}H NMR spectrum of **2** (500 MHz, room temperature), obtained by the addition of 1 equiv of NaOH (dissolved in 1a minimum amount of D_2O) to the DMSO-d_6 solution of **1a**.

7.15 ^{13}C{^{1}H} NMR spectrum of 2 in DMSO-d_6

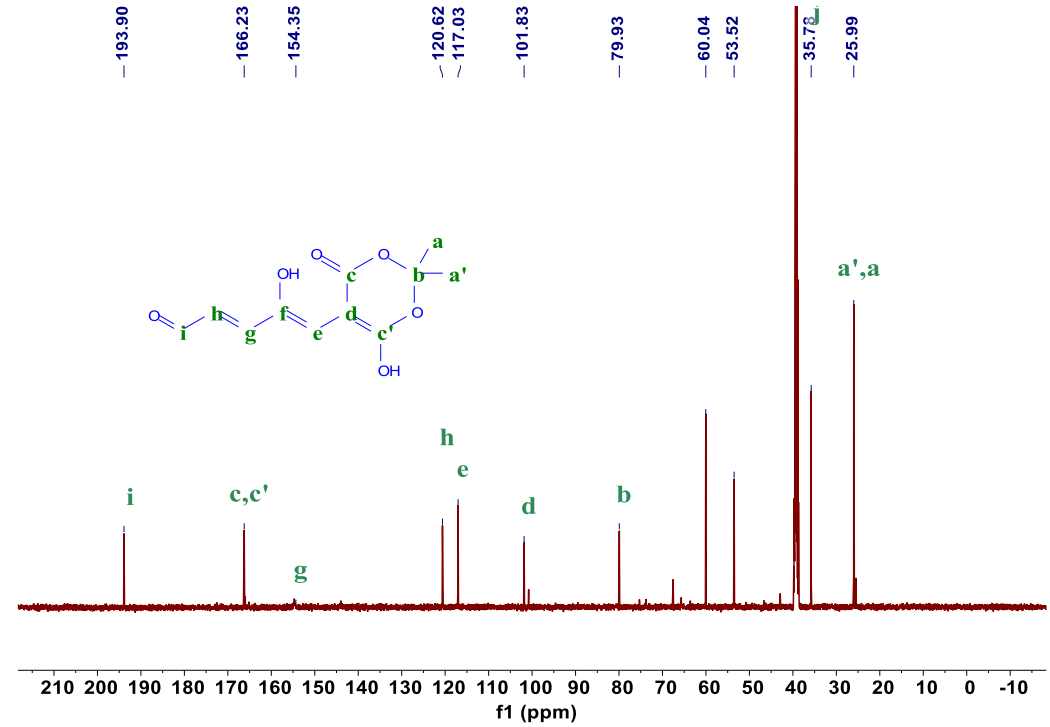

Figure S35. ^{13}C{^{1}H} NMR spectrum of **2** (125 MHz, room temperature), obtained by the addition of 1 equiv of NaOH (dissolved in 1a minimum amount of D_2O) to the DMSO-d_6 solution of **1a**.

7.16 ^{1}H, ^{1}H–COSY NMR spectrum of 2 in DMSO-d_6

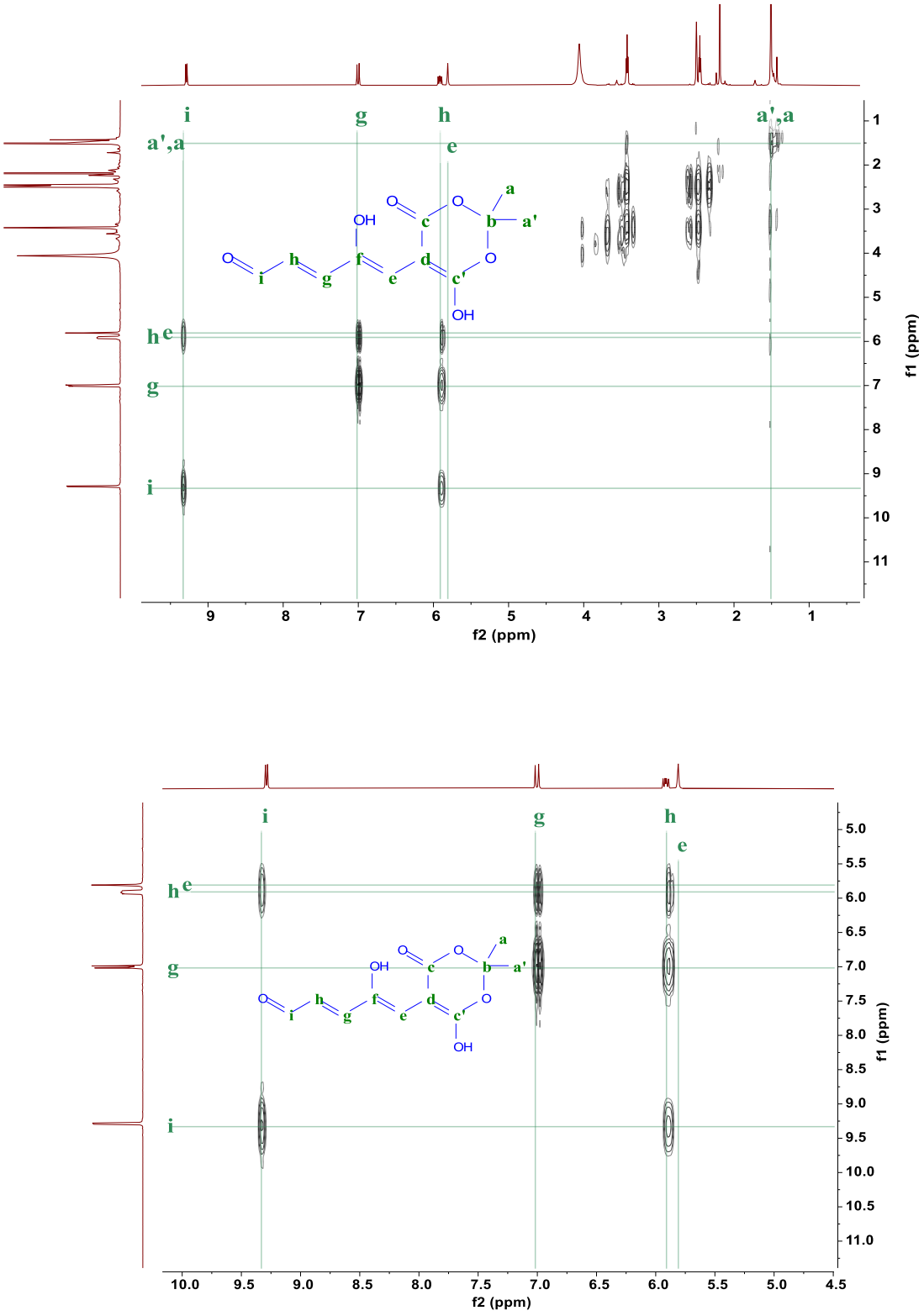

Figure S36. Entire (top) and zoomed (bottom) ^{1}H, ^{1}H–COSY NMR spectra of **2** in DMSO-d_6 (500 MHz, room temperature).

7.17 HSQC NMR spectrum of 2 in DMSO-d_6

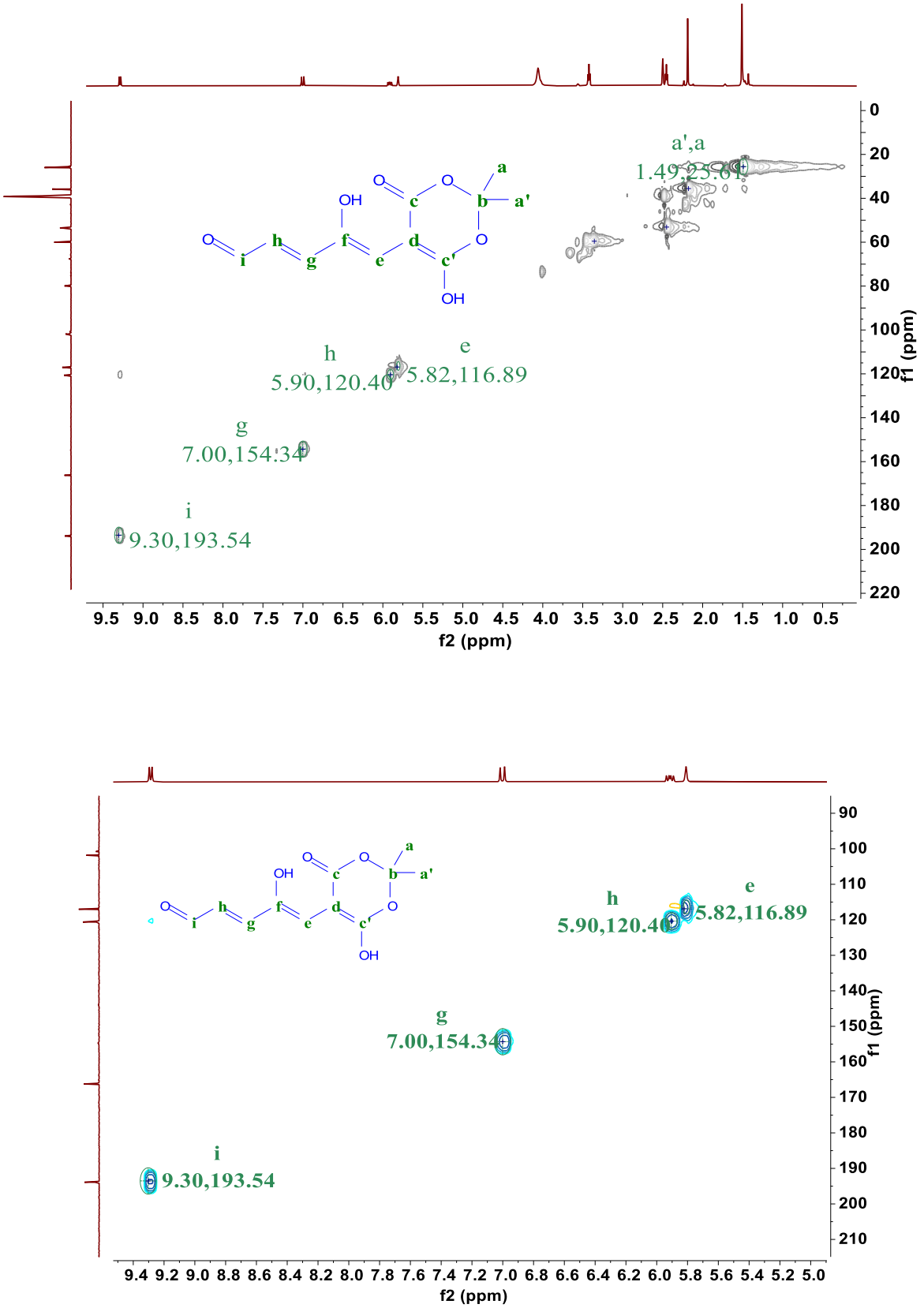

Figure S37. Entire (top) and zoomed (bottom) HSQC NMR spectra of **2** in DMSO-d_6 (500 MHz, room temperature).

7.18 NOESY NMR spectrum of 2 in DMSO-d_6

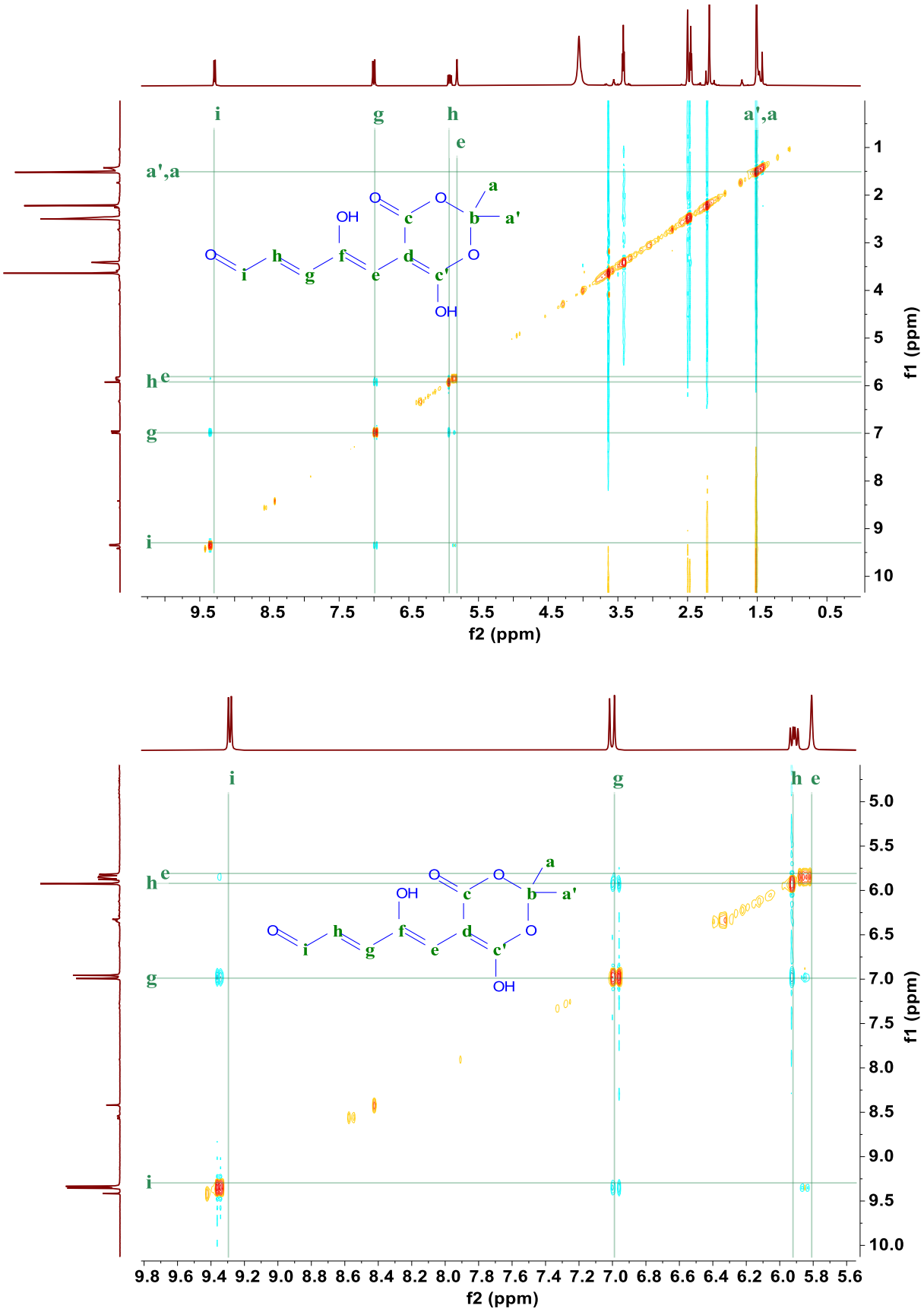

Figure S38. Entire (top) and zoomed (bottom) NOESY NMR spectra of **2** in DMSO-d_6 (400 MHz, room temperature).

7.19 ^{1}H NMR spectrum of 1d in D_2O.

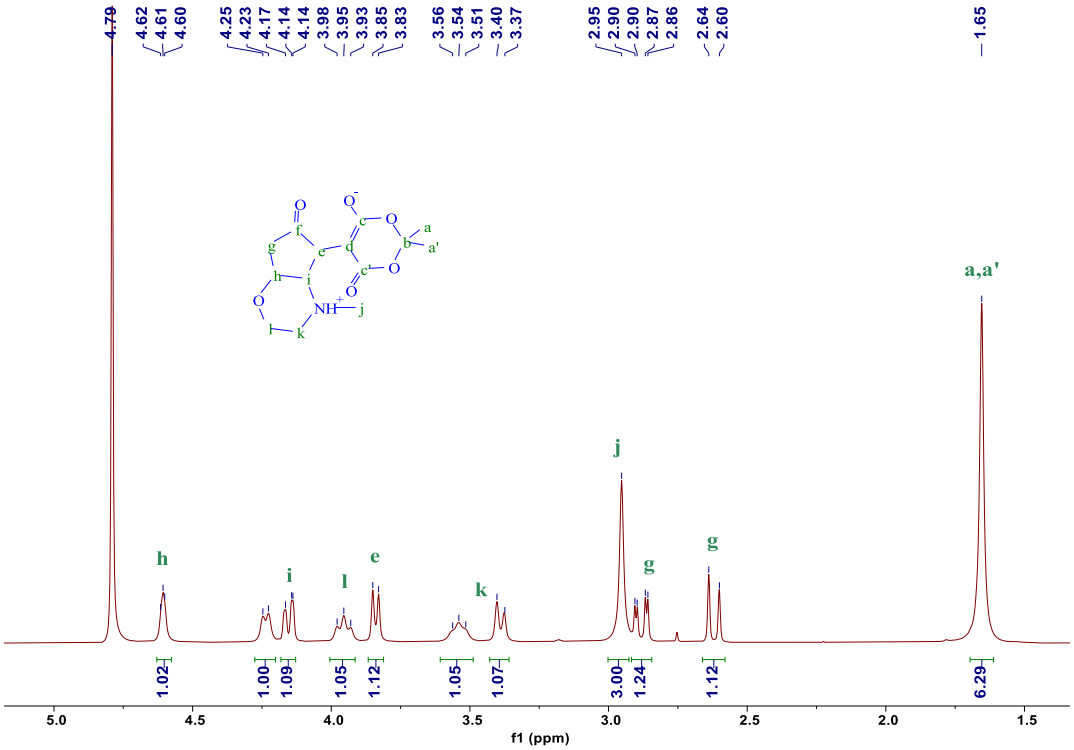

Figure S39. ^{1}H NMR spectrum of **1d** in D_2O (500 MHz, room temperature).

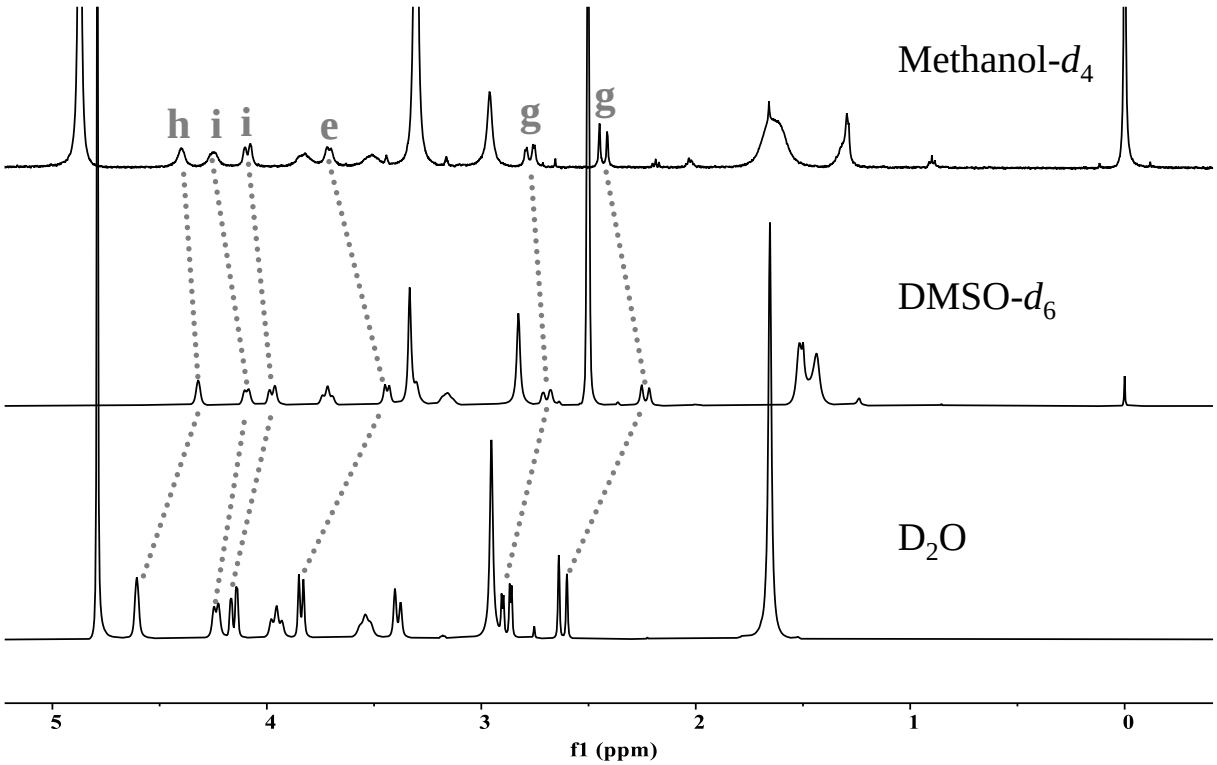

Figure S40. Stacked ^{1}H NMR spectra of **1d** in D_2O, DMSO-d_6, and methanol-d_4 (freshly dissolved, 500 MHz, room temperature).

7.20 $^{13}C\{^{1}H\}$ NMR spectrum of 1d in D_2O

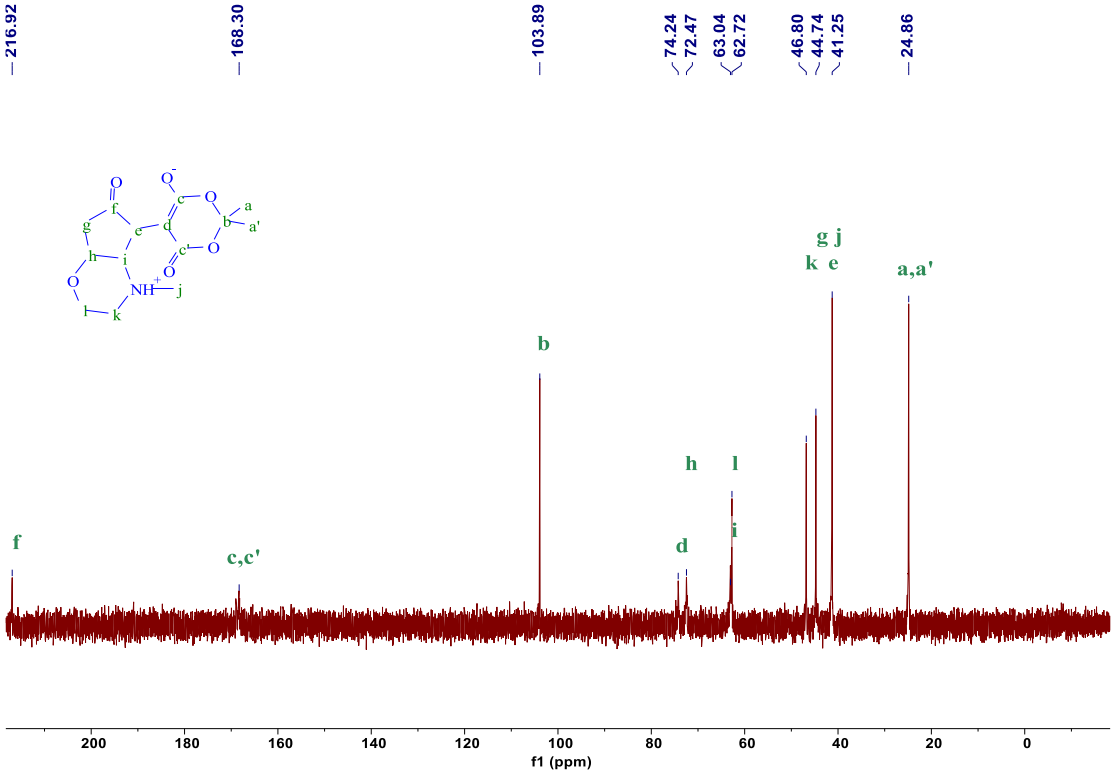

Figure S41. $^{13}C\{^{1}H\}$ NMR spectrum of **1d** in D_2O (125 MHz, room temperature).

7.21 ^{1}H, ^{1}H–COSY NMR spectrum of 1d in D_2O

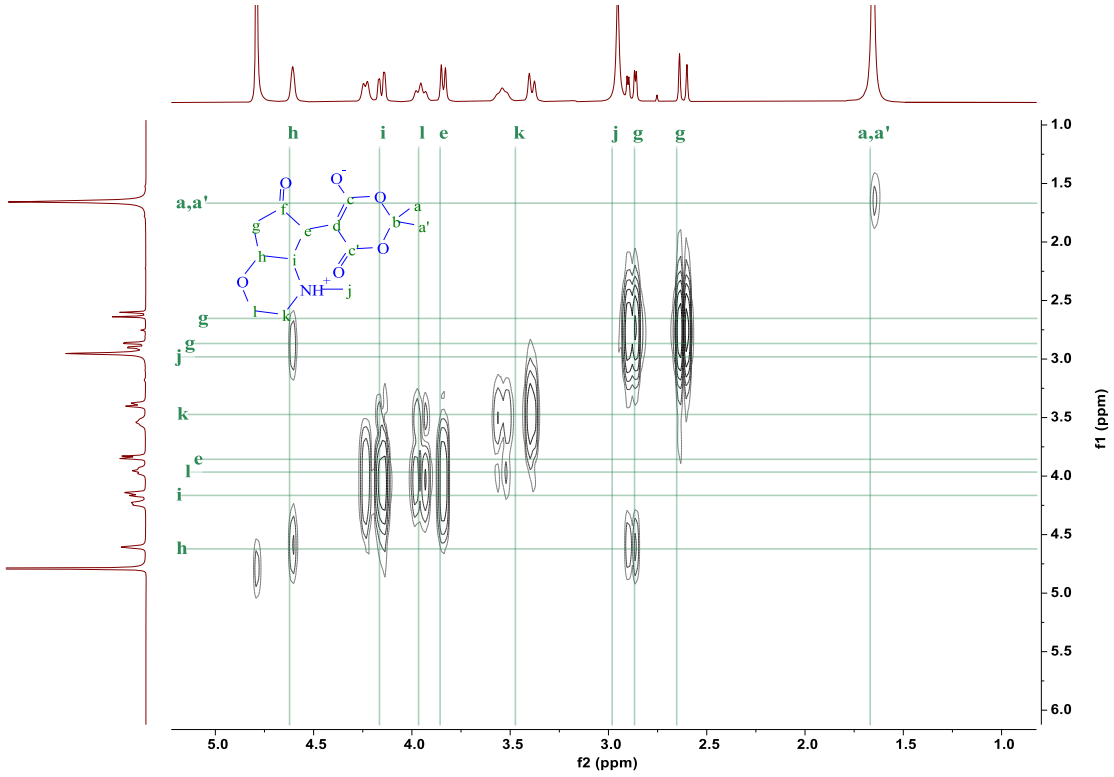

Figure S42. ^{1}H, ^{1}H-COSY NMR spectrum of **1d** in D_2O (500 MHz, room temperature).

7.22 HSQC NMR spectrum of 1d in D_2O

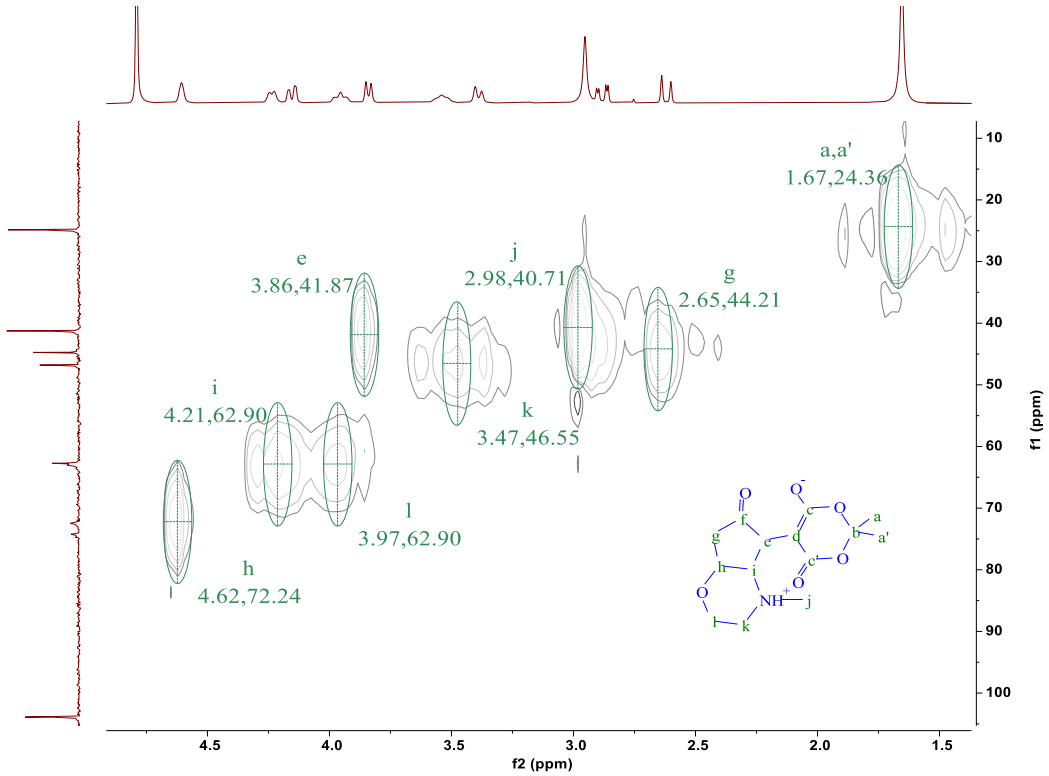

Figure S43. HSQC spectrum of **1d** in D_2O (500 MHz, room temperature).

8. Mass spectrum

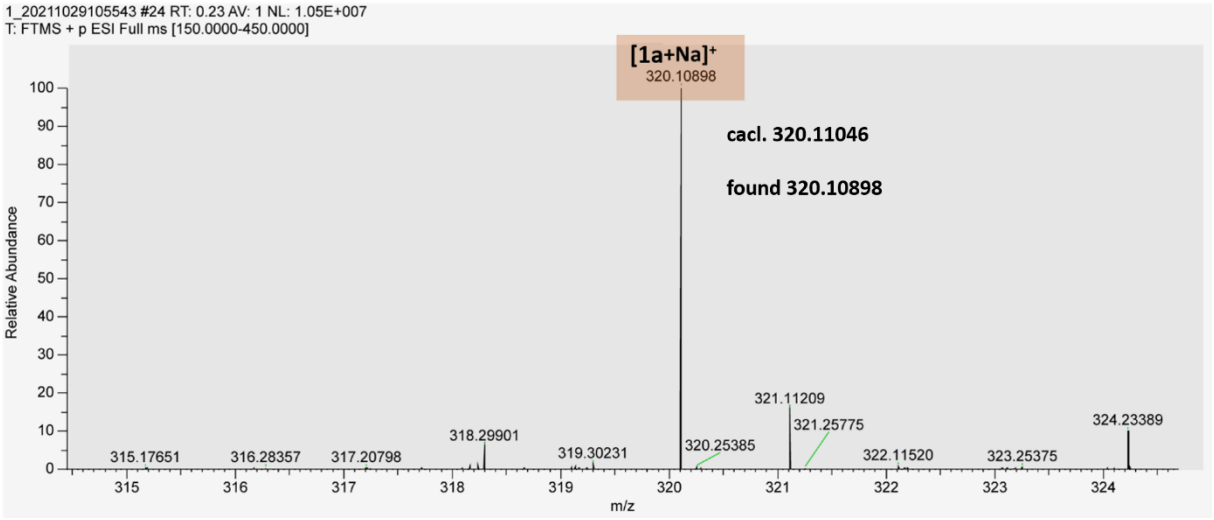

Figure S44. Mass spectrum (ESI) of **1a** in MeOH. The calculated and experimental signals for **[1a+Na]**$^+$ are as indicated.

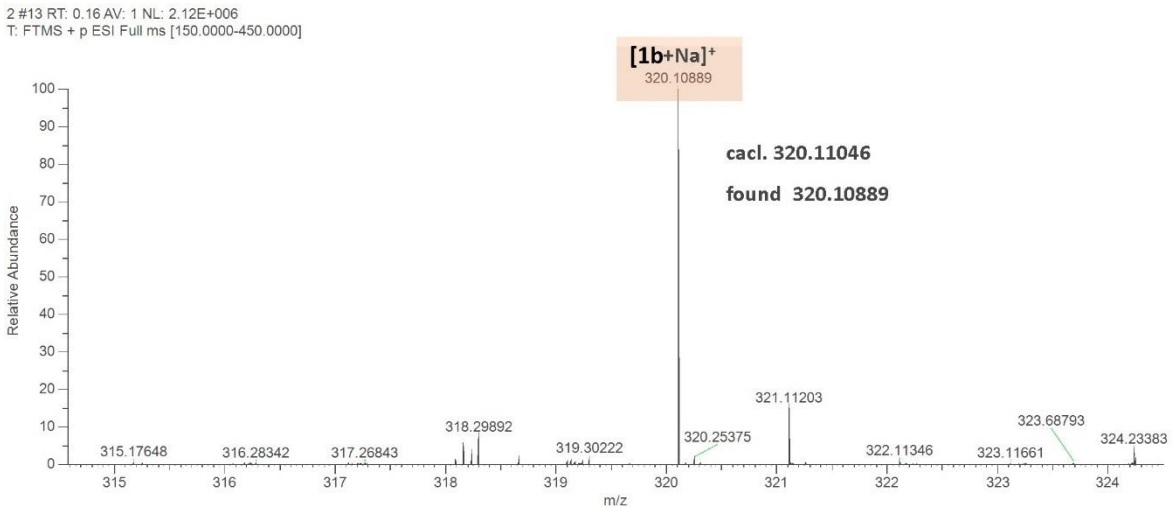

Figure S45. Mass spectrum (ESI) of **1b** in MeOH. The calculated and experimental signals for **[1b+Na]**$^+$ are as indicated.

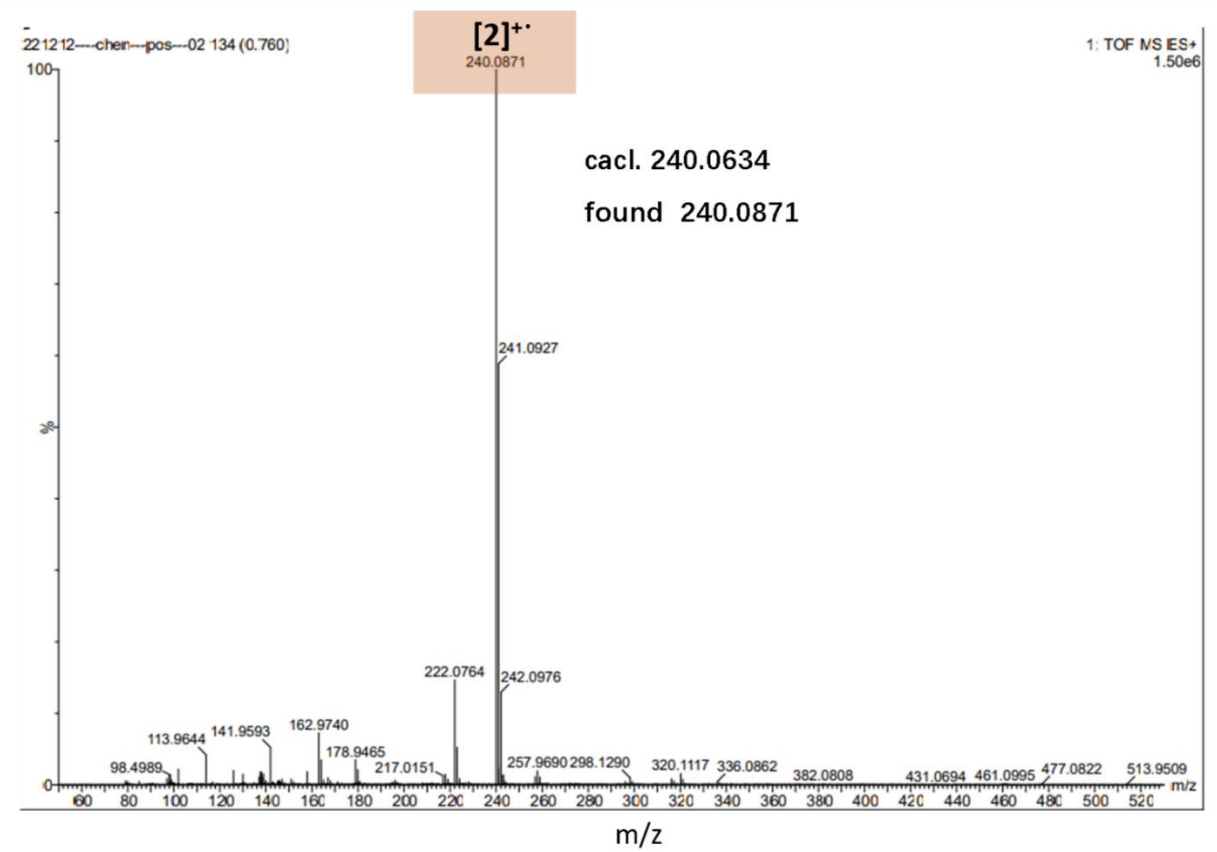

Figure S46. Mass spectrum (ESI) of **2** in MeOH. The calculated and experimental signals for **[2]**$^{+\cdot}$ are as indicated.

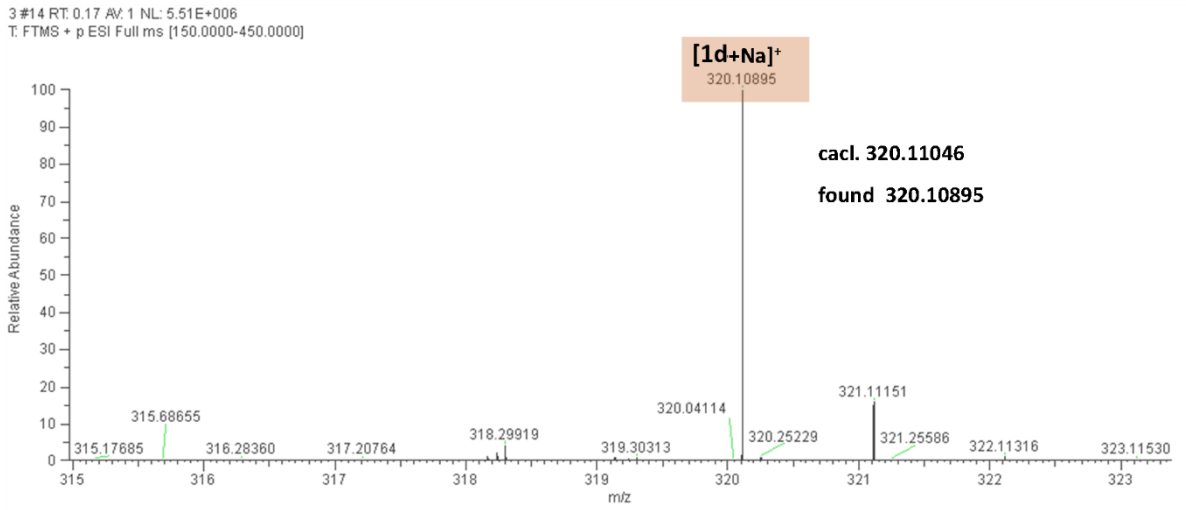

Figure S47. Mass spectrum (ESI) of **1d** in MeOH. The calculated and experimental signals for **[1d+Na]**$^+$ are as indicated.

9. Crystal data and refinement details

Table S4. Crystal data and refinement details for **1d**.

Temperature / K	298
Empirical formula	$C_{14}H_{19}NO_6$
Formula weight / g mol^{-1}	297.30
Crystal system	orthorhombic
Space group	*Pca2$_1$*
a / Å	17.469(5)
b / Å	7.599(2)
c / Å	11.007(3)
β / °	90
Volume / Å^3	1461.2(7)
Z	4
ρ_{calc} / mg mm^{-3}	1.351
μ / mm^{-1}	0.106
F(000)	632.0
Reflections collected	13781
Independent reflections	3349
R_{int}	R_{int} = 0.0378
Goodness-of-fit on F^2	1.028
Final *R* indexes[a] [$I \geq 2\sigma(I)$] Final *R* indexes [all data] Largest diff. peak/hole / eÅ^{-3}	R_1 = 0.0368 wR_2 =0.0716 R_1 = 0.0573 wR_2 = 0.0781 0.12/-0.11

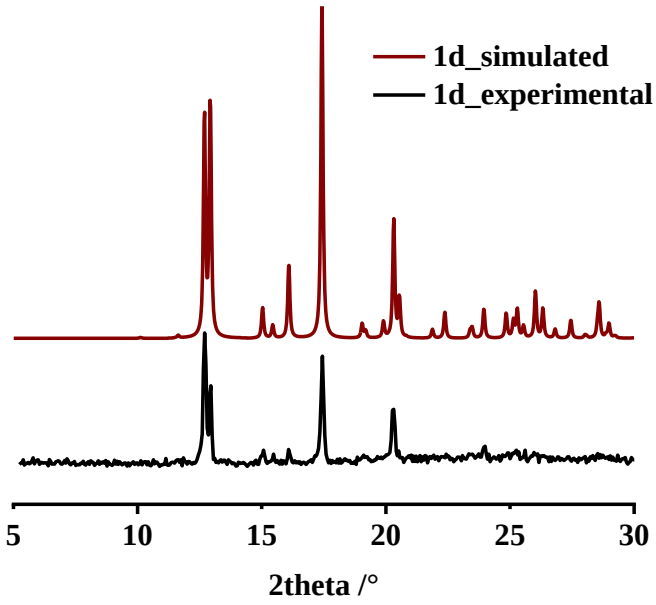

Figure S48. Experimental and simulated PXRD patterns of **1d**.

10. References

1. G. M. Sheldrick, *Acta Crystallographica a-Foundation and Advances*, 2008, **64**, 112-122.
2. O. V. Dolomanov, L. J. Bourhis, R. J. Gildea, J. A. K. Howard and H. Puschmann, *J. Appl. Crystallogr.*, 2009, **42**, 339-341.
3. S. Helmy, S. Oh, F. A. Leibfarth, C. J. Hawker and J. Read de Alaniz, *J. Org. Chem.*, 2014, **79**, 11316-11329.
4. N. Mallo, E. D. Foley, H. Iranmanesh, A. D. W. Kennedy, E. T. Luis, J. Ho, J. B. Harper and J. E. Beves, *Chem Sci*, 2018, **9**, 8242-8252.
5. C. Reichardt, *Chem. Rev.*, 1994, **94**, 2319-2358.
6. M. M. Sroda, F. Stricker, J. A. Peterson, A. Bernal and J. Read de Alaniz, *Chemistry*, 2021, **27**, 4183-4190.
7. M. M. Lerch, M. Di Donato, A. D. Laurent, M. Medved, A. Iagatti, L. Bussotti, A. Lapini, W. J. Buma, P. Foggi, W. Szymański and B. L. Feringa, *Angew. Chem. Int. Ed.*, 2018, **57**, 8063-8068.
8. M. M. Lerch, M. Medved, A. Lapini, A. D. Laurent, A. Iagatti, L. Bussotti, W. Szymanski, W. J. Buma, P. Foggi, M. Di Donato and B. L. Feringa, *J. Phys. Chem. A*, 2018, **122**, 955-964.
9. S. Singh, K. Friedel, M. Himmerlich, Y. Lei, G. Schlingloff and A. Schober, *ACS Macro Lett*, 2015, **4**, 1273-1277.
10. A. Boulmier, M. Haouas, S. Tomane, L. Michely, A. Dolbecq, A. Vallee, V. Brezova, D. L. Versace, P. Mialane and O. Oms, *Chemistry*, 2019, **25**, 14349-14357.